The net charge of the K-loop regulates KIF1A superprocessivity by enhancing microtubule affinity in the one-head-bound state

Taylor M. Zaniewski[1] and William O. Hancock[2]

Departments of [1]Chemistry and [2]Biomedical Engineering, Pennsylvania State University, University Park, Pennsylvania, USA

Acknowledgements:

The authors thank Dr. Kristen Verhey for helpful discussions that resolved differences between the current results and previously published KIF1A data. The authors thank the Hancock lab group members for their helpful discussions, with particular thanks to Adheshwari Ramesh and Samira Bell for their help making the plasmids used in this study.

Abstract:

KIF1A is an essential neuronal transport motor protein known for its superprocessive motility. We determined that superprocessivity of KIF1A dimers originates from a unique structural domain, the lysine rich insertion in loop-12 termed the 'K-Loop', which enhances electrostatic interactions between the motor and the microtubule. In 80 mM PIPES buffer, replacing the native loop-12 of KIF1A with that of kinesin-1, resulted in a 6-fold decrease in run length, and adding additional positive charge to loop-12 enhanced the run length. Interestingly, swapping the KIF1A loop-12 into kinesin-1 did not enhance its run length, consistent with the two motor families using different mechanochemical tuning to achieve persistent transport. To investigate the mechanism by which the KIF1A K-loop enhances processivity, we used microtubule pelleting and single molecule dwell times assays in ATP and ADP. First, the microtubule affinity was similar in ATP and in ADP, consistent with the motor spending the majority of its cycle in a weakly-bound state. Second, the microtubule affinity and single-molecule dwell time in ADP were 6-fold lower in the loop-swap mutant compared to the wild type. Thus, the positive charge in loop-12 of KIF1A enhances the run length by stabilizing the motor binding in its vulnerable one-head-bound state. Finally, through a series of mutants with varying positive charge in the K-loop, we found that the KIF1A processivity is linearly dependent on the charge of loop-12.

Introduction

KIF1A is a fast and superprocessive neuronal transport motor protein in the kinesin-3 family that is responsible for the delivery of synaptic vesicle precursors from the soma to the distal end of the axon, among other tasks.[1–5] Genetic mutations lead to KIF1A Associated Neurological Disorders (KAND), rare and often misdiagnosed afflictions.[5–14] The category of KAND is vast, with 113 variants that have been identified in humans so far, making therapeutic attempts difficult.[15] Therefore, approaching treatments more systematically requires a deeper understanding of the fundamental mechanochemical mechanism of KIF1A.

A recent biochemical dissection of the KIF1A chemomechanical cycle concluded that: i) both ATP binding and hydrolysis are required to trigger tethered-head binding, ii) rear head detachment is fast and may contribute to the fast stepping rate, and iii) the motor spends the majority of its stepping cycle in a post-hydrolysis, one-head-bound (1HB) state.[16] This ability to remain associated with the microtubule in a "weakly-bound" state enhances the motor processivity by ensuring that the motor remains bound to the microtubule sufficiently long for the tethered head to complete its step and bind to the next site.[17–19] This property of remaining in a vulnerable one-head-bound state also provides an explanation for the propensity of KIF1A to detach readily under load.[20–23] A recent optical trapping study that used a three-bead geometry to minimize forces oriented perpendicular to the microtubule concluded that under load KIF1A is able to sustain loads by rapidly rebinding to the microtubule following disengagement.[21] Because KIF1A does not achieve high microtubule affinity by maximizing the duration spent in a strong binding two-head-bound state, we proposed that the source of its processivity is a combination of a relatively slow detachment rate from the post-hydrolysis 1HB state and faster tethered-head attachment rate compared to kinesin-1 and -2.[16] The goal of the current study was to define the structural elements of KIF1A that underlie this kinetic tuning.

The kinesin-3 family is known for a unique structural domain called the K-Loop. This domain is a stretch of Loop-12 in which KIF1A has six lysine residues and kinesin-1 and -2 only have one lysine.[24] In early work it was determined that the electrostatic interaction of the K-Loop with the microtubule facilitates diffusive motion, leading to monomeric motility of KIF1A.[24–26] The

enhanced positive charge of KIF1A in this region is thought to interact with the glutamate rich C-terminal tail of tubulin, termed the 'E-hook'.[27,28] However, because these domains are disordered, and their structures and interactions not resolved by X-ray crystallography or CryoEM, [28–30] biochemical and single-molecule investigations are vital for understanding this interaction.

In the literature, there are conflicting reports of the role of the K-loop in KIFA superprocessivity, with some studies indicating that the K-loop is responsible for KIF1A superprocessivity, [27,31] and others suggesting that the K-loop plays no role in the processivity of KIF1A and only increases its microtubule on-rate.[32] This lack of consensus in the field has led to considerable confusion regarding the role of the K-loop in long distance intracellular transport. In the present study, we used single-molecule microscopy and stopped-flow biochemical experiments to clarify the role of loop-12 in KIF1A motility. By using a series of mutations, buffers, and experimental approaches, we determined that at near physiological ionic strength the K-loop enhances the processivity of KIF1A by strengthening the microtubule affinity of a vulnerable one-head-bound state in the KIF1A chemomechanical cycle. Additionally, this functionality cannot be transferred to kinesin-1, highlighting how different motor families use distinct biochemical tuning to achieve fast and processive motility.

Results

Influence of the neck-coil and coiled-coil domains on KIF1A motility

To understand how different structural elements of KIF1A contribute to its motility and to reconcile conflicting results in the literature, we designed constitutively active constructs of KIF1A that included different distal coiled-coil domains to ensure stable KIF1A dimers and included or excluded the native neck-coil domain of KIF1A. All of the KIF1A constructs are based on a truncated and constitutively active KIF1A dimer that has been used in a number of published studies.[16,27,32,33] The 'neck coil', defined as residues 369-393 of *Rattus norvegicus* KIF1A, is a short coiled-coil domain that is immediately distal to the disordered neck linker domain and is involved in dimerization of the two motor domains.[34,35] Based on other members of the kinesin-3 family, it is thought that in full-length KIF1A, coiled-coil 1 folds back on the neck-coil and forms an antiparallel coiled-coil that separates the two heads and inhibits motor activity.[33,34] It was shown previously that the neck-coil alone is insufficient to stably dimerize KIF1A,[33–35] and that this could be rectified by adding a leucine zipper (LZ) downstream of the neck-coil.[20,27,33] A second approach to dimerizing diverse kinesins has been to fuse the motor and neck linker domains to the neck-coil of *D. melanogaster* kinesin-1 (KHC residues 345 to 406), which was shown previously to form a stable dimerization domain, or to the neck-coil plus coiled-coil 1 (KHC residues 345 to 560).[16,18,36–38]

To directly compare how these different dimerization strategies affect KIF1A motility, we designed three dimeric, GFP-tagged *Rattus norvegicus* KIF1A constructs, as follows. The first construct consisted of KIF1A residues 1-393 followed by a leucine zipper domain and GFP (KIF1A(1-393)-LZ-GFP), which we refer to as $1A_{393}$-LZ (**Error! Reference source not found.**A). This construct matches those used in a number of published studies, albeit with different C-terminal tags.[20,27,31,33] We made two other constructs that achieved stable dimerization through the *Drosophila melanogaster* kinesin heavy chain (KHC) neck-coil and coiled-coil 1 domains (345-560). The first construct, which included the KIF1A neck-coil, was KIF1A(1-393)-K560-GFP, referred to as $1A_{393}$ (Fig. 1A-B). The second construct, which did not include the KIF1A neck coil and was used in a previous study,[16] was KIF1A(1-368)-K560-GFP, referred to as $1A_{368}$ (Fig. 1A).

The first question we addressed was whether the dimerization strategy affected the KIF1A run length in 80 mM PIPES (BRB80) buffer. We found that $1A_{393}$-LZ had a 2-fold longer run length than $1A_{393}$ (6.1 ± 0.1 and 3.0 ± 0.02 μm, respectively; Fig. 1C with raw data in Fig. S1). We propose that this difference in processivity is due to the differential charge in the coiled-coil domains. The net charge of coil-1 of KIF1A, which these dimerization domains replace, is -6; the net charge of the kinesin-1 neck-coil (345-405) is -3; and the net charge of the leucine zipper is +1 (Fig. S2). Because the run length is influenced by the motor's affinity to the negatively charged microtubule, the most likely explanation is that the run length differences result from different electrostatic interactions with the microtubule.[39] To probe whether these different dimerization strategies also lead to different microtubule affinities in the weak-binding ADP state of KIF1A, we used TIRF microscopy to measure the microtubule dwell time of the two constructs in saturating ADP. Consistent with the run length differences, $1A_{393}$-LZ had a ~3-fold longer dwell time than $1A_{393}$ (**Error! Reference source not found.**F). Thus, because the negative net charge of the Kin1 neck coil sequence, and because this domain has been used in a body of our previous work, we focused our efforts on the $1A_{393}$ construct.

Because the KIF1A neck-coil domain has been shown to be insufficient to form a stable dimer on its own,[33] it is possible that even in constructs dimerized by fusing a distal coiled-coil domain, the neck-coil does not form a stable connection between the two motor domains. This 'breathing' of the neck-coil could affect the interhead coordination necessary for processivity, consistent with previous work that showed extending the length of the kinesin neck linker reduced motor run lengths.[35,40–42] To test whether the KIF1A neck-coil plays a role beyond dimerization, we used TIRF microscopy in BRB80 buffer to compare the run length of $1A_{393}$, which includes the neck-coil, to $1A_{368}$, which lacks the neck-coil (Fig. 1A). The two constructs had similar run lengths, indicating that the sequence and stability of the KIF1A neck-coil has no effect on its processivity (**Error! Reference source not found.** B, D). Consistent with the run lengths, the microtubule dwell times of the two motors in 2 mM ADP, which probes the affinity in the weak-binding state, were also similar (Fig. 1G). We hypothesized that if there is any reversible dimerization in the KIF1A neck-coil, then it may have a stronger effect on kinesin-1, which has a shorter neck linker domain and thus a stiffer connection between the two heads than KIF1A.[18,41–44] To test this, we used *Drosophila* kinesin-1 truncated at residue 560 and fused to GFP (KHC(1-560)-GFP, referred

to as Kin1).[16,18,36,37] The KIF1A neck-coil domain (KIF1A 369-393) was inserted just upstream of Ala_{345} at the start of the neck-coil of Kin1 to generate $K1_{1Anc}$ (Fig. 1A). [45] In single molecule assays, the Kin1 run length was 0.8 ± 0.02 μm/s (Fig. 1E), which is consistent with previous work and is four-fold shorter than KIF1A Fig. 1C).[18,36,37] $K1_{1Anc}$ had a ~2-fold shorter run length than Kin1 (0.4 ± 0.002 μm; **Error! Reference source not found.** D) and also had a slightly slower velocity (0.5 ± 0.2 μm/s versus 0.7 ± 0.2 μm/s; **Error! Reference source not found.**E). This result suggests that the KIF1A neck-coil dimerizes only weakly, and acts as an extended neck linker in kinesin-1, reducing its performance.[18,41–43] A possible explanation for the lack of neck-coil effects in KIF1A is that its native neck linker is already longer and thus more flexible than kinesin-1. It follows that the superprocessivity of KIF1A does not result from tight mechanical connection between the heads to achieve coordinated stepping, but rather from other aspects of the motor's chemomechanics.

Influence of ionic strength on KIF1A motility

To better understand the role of electrostatic interactions in KIF1A motility and to reconcile diverse studies across the literature, we investigated the effect of buffer ionic strength on KIF1A motility. We chose two buffers commonly used in the literature: BRB80, which contains 80 mM PIPES and has a 173 mM ionic strength, and BRB12, which contains 12 mM PIPES and has a 26 mM ionic strength (both buffers also include 1 mM $MgCl_2$, 1 mM EGTA, pH 6.9). Although much of the published work on KIF1A was performed in BRB12,[20,27,32,33] the ionic strength of BRB80 (173 mM) is closer to the ~200 mM ionic strength estimated in cells.[46] The low ionic strength of BRB12 is expected to maximize electrostatic interactions between motors and microtubules; for instance, the Debye length in BRB80 is 0.7 nm in BRB80 and 2 nm in BRB12.[47]

Consistent with enhanced electrostatic interactions, we found that $1A_{393}$ had a nearly 5-fold longer run length in BRB12 compared to BRB80 (14.3 ± 0.4 μm versus 3.0 ± 0.02; Fig. 1C). Additionally, we observed increased pausing behavior at low ionic strength, as reported previously.[27] Thus, we quantified the segmented velocity (**Error! Reference source not found.**D) and found that the velocity decreased from 1.5 μm/s in BRB80 to 1.1 μm/s in BRB12. The longer run length and slower velocity correspond to a substantially higher affinity of KIF1A for microtubules in BRB12 buffer. To compare the microtubule affinity of KIF1A in its weak-binding ADP state in these

different buffers, we measured the microtubule dwell time in 2 mM ADP and found that the dwell time in BRB12 was 10-fold longer than in BRB80 (**Error! Reference source not found.**F). Thus, the enhanced run length of KIF1A in BRB12 can be explained by the reduced charge shielding at lower ionic strength enhancing the electrostatic interaction between the microtubule and KIF1A in the weakly-bound ADP state. Because these enhanced electrostatic interactions in BRB12 may mask other aspects of KIF1A mechanochemistry, we focused our efforts on characterizing KIF1A in BRB80, which is closer to physiological ionic strength.

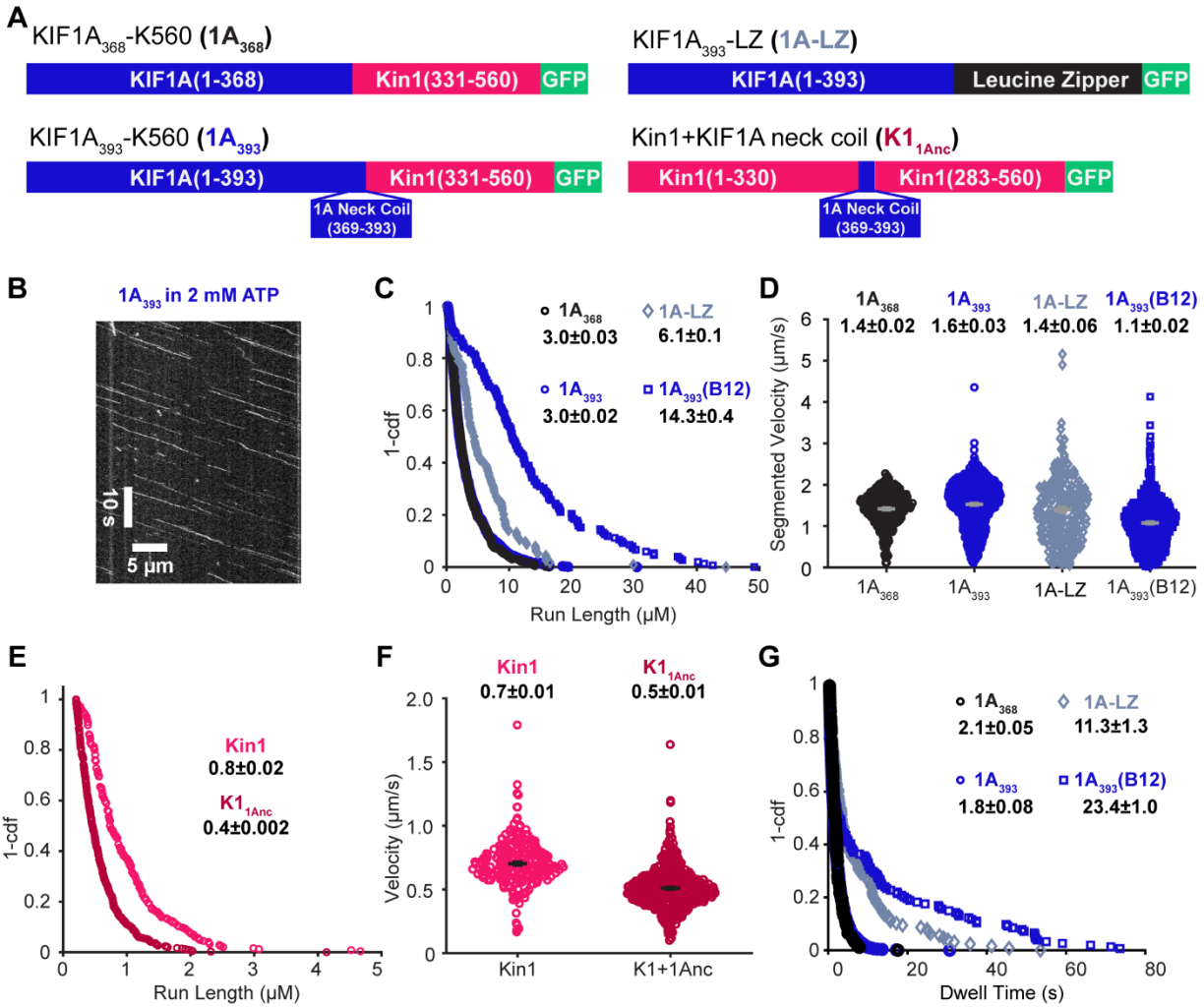

Figure 1: **Dimerization domain and ionic strength of buffer impact KIF1A motility**

A, Diagrams of the protein constructs used in this study. KIF1A refers to *Rattus norvegicus* KIF1A; KHC refers to *Drosophila melanogaster* Kinesin heavy chain. **B,** Example kymograph of $1A_{393}$ in 2 mM ATP and BRB80. Scale bars are 10 sec and 5 µm. **C,** Run length distribution of $1A_{368}$ (black circles), $1A_{393}$ (blue circles), $1A_{393}$-LZ (navy diamonds), and $1A_{393}$ in BRB12 (blue

squares). Single exponential fits give run lengths of 3.0 ± 0.03, 3.0 ± 0.02, 6.1 ± 0.1, and 14.3 ± 0.4 μm, respectively (fit ± 95% confidence interval). **D,** Velocity distribution of $1A_{368}$ (black circles), $1A_{393}$ (blue circles), $1A_{393}$-LZ (navy diamonds), and $1A_{393}$ in BRB12 (blue squares). Average segmented velocities are 1.4 ± 0.02, 1.6 ± 0.03, 1.4 ± 0.06, 1.1 ± 0.02 μm/s, respectively (mean ± SEM). **E,** Run length distribution of Kin1 (pink) and $K1_{1Anc}$ (red). Single exponential fits give run lengths of 0.8 ± 0.02, and 0.4 ± 0.002 μm, respectively (fit ± 95% confidence interval). **F,** Velocity distribution of Kin1 (pink) and $K1_{1Anc}$ (red). Average velocities are 0.7 ± 0.2 and 0.5 ± 0.2 μm/s, respectively (mean ± SD). **G,** Dwell time distributions in 2 mM ADP. Single exponential fits to $1A_{368}$ (black circles) and $1A_{393}$ (blue circles) give dwell times of 2.1 ± 0.05 and 1.8 ± 0.08 s, respectively. $1A_{393}$-LZ (navy diamonds) and $1A_{393}$ in BRB12 (blue squares) were fit with biexponentials. $1A_{393}$-LZ had dwell times of 2.0 ± 0.3 and 11.3 ± 1.3 s, and $1A_{393}$ in BRB12 had dwell times of 1.1 ± 0.04 and 23.4 ± 1.0 s; the longer duration for each is presented in the figure.

K-loop regulates the run length of KIF1A but not Kin-1

Earlier studies of KIF1A monomers found that the positively charged Loop-12 of KIF1A enhances its microtubule affinity,[24] however subsequent studies of KIF1A dimers have reported Loop-12 does not contribute to superprocessivity.[32] To test whether the K-Loop is responsible for the superprocessivity of our KIF1A construct in BRB80 buffer, we examined the properties of a 'swap' construct, in which the native loop-12 of KIF1A is removed and replaced with the kinesin-1 loop-12, KIF1A(1-393)-Kin1Loop12-K560-GFP (referred to as 1A-K1L12; **Error! Reference source not found.**A).[24,32] Swapping out the KIF1A Loop-12 caused a 6-fold decrease in the run length and a slight decrease in velocity, consistent with Loop-12 being the determinant of KIF1A superprocessivity (Fig. 2 B-C and Fig. S3).

If Loop-12 is enhancing KIF1A processivity by enhancing electrostatic interactions with the microtubule, then in principle swapping it into kinesin-1 should enhance the run length, and previous work found this to be the case in low ionic strength buffer.[32] To test this question in BRB80 buffer where physiological charge shielding is expected, we made a 'reverse swap' mutant, in which the KIF1A loop-12 was inserted into kinesin-1, replacing the native loop-12 (referred to

as K1-1AL12; **Error! Reference source not found.**A). Surprisingly, inserting the positively charged KIF1A K-loop into Kin-1 did not impact the velocity or run length (Fig. 2E-F; see Fig. S3 for representative kymographs). Thus, due to differences in the microtubule binding interface and/or kinetic tuning of kinesin-1, adding the positively charged K-loop into kinesin-1 does not enhance its processivity in near physiological ionic strength buffer.

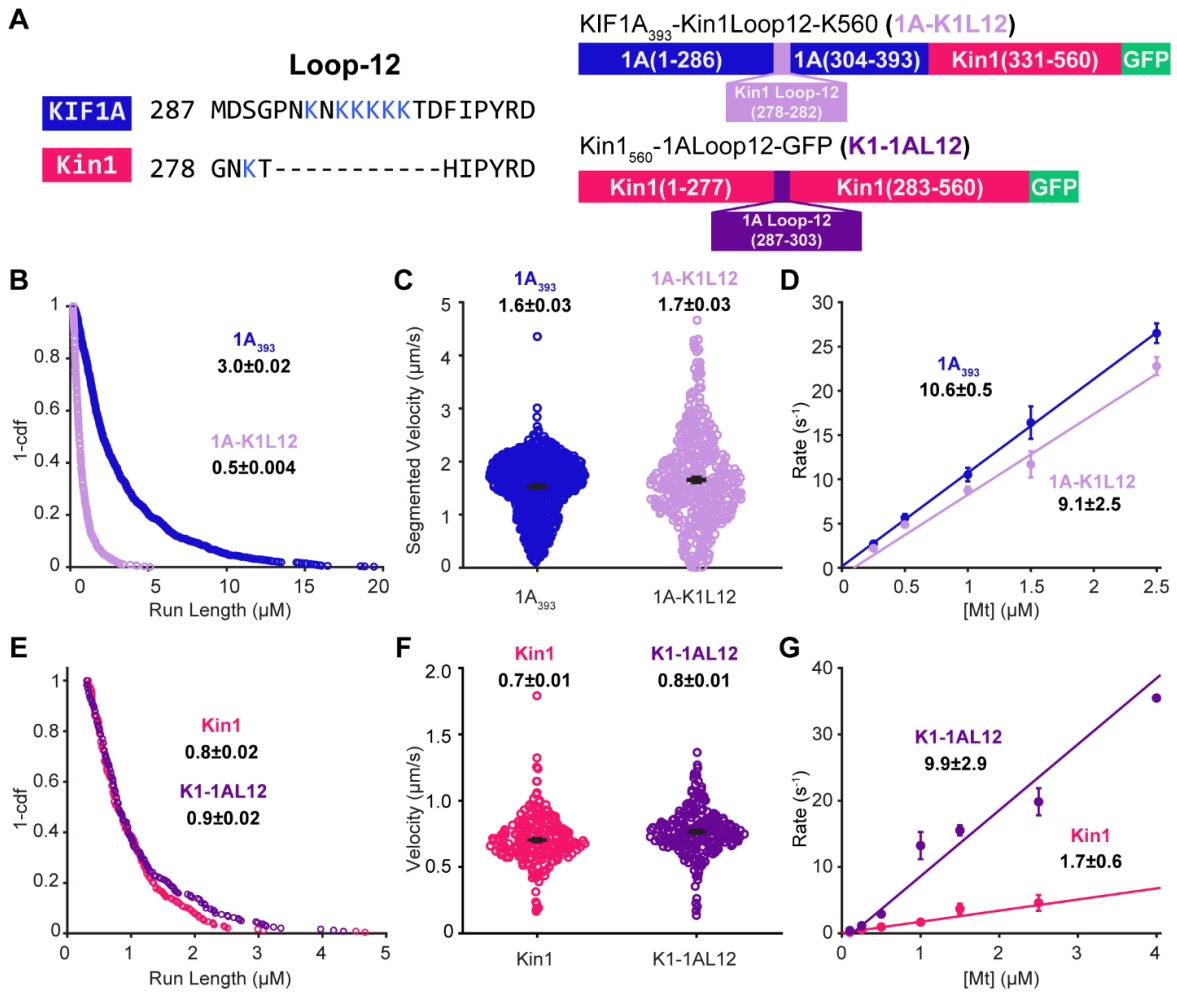

Figure 2: **K-Loop is the source of KIF1A superprocessivity**

A, Diagrams of the loop swap constructs. **B,** Run length distribution of $1A_{393}$ (blue circles) and 1A-K1L12 (light purple circles) in BRB80 and 2 mM ATP. Single exponential fits give run lengths of 3.0 ± 0.02 and 0.5 ± 0.004 μm, respectively (fit ± 95% confidence interval). **C,** Velocity distribution of $1A_{393}$ (blue circles) and 1A-K1L12 (light purple circles) in BRB80 and 2 mM ATP. Average segmented velocities are 1.6 ± 0.03 and 1.7 ± 0.03 μm/s, respectively (mean ± SEM). P<0.0001 **D,** Bimolecular on-rates of $1A_{393}$ (blue circles) and 1A-K1L12 (light purple circles).

Linear fits give k_{on}^{Mt} of 10.6 ± 0.5 and 9.1 ± 2.5 $\mu M^{-1}s^{-1}$, respectively (fit ± 95% confidence interval). Points are mean ± SEM. **E,** Run length distribution of Kin1 (pink circles) and K1-1AL12 (dark purple circles) in BRB80 and 2 mM ATP. Single exponential fits give run lengths of 0.8 ± 0.02 and 0.9 ± 0.02 μm, respectively (fit ± 95% confidence interval). **F,** Velocity distribution of Kin1 (pink circles) and K1-1AL12 (dark purple circles) in BRB80 and 2 mM ATP. Average velocities are 0.7 ± 0.01 and 0.8 ± 0.01 μm/s, respectively (mean ± SEM). P<0.0001 **G,** Bimolecular on-rates of Kin1 (pink circles) and K1-1AL12 (dark purple circles). Linear fits give k_{on}^{Mt} of 1.7 ± 0.6 and 9.9 ± 2.9 $\mu M^{-1}s^{-1}$, respectively (fit ± 95% confidence interval). Points are mean ± SEM.

To further investigate how positive charge in loop-12 differentially affects KIF1A and kinesin-1, we compared the effects of the loop swap on the microtubule on-rate of the two motors. Using stopped-flow, the bimolecular on-rate (k_{on}^{Mt}) was measured by incubating the motors with fluorescently labeled mant-ADP in BRB80 and flushing the solution against varying concentrations of taxol-stabilized microtubules in 2 mM ADP. Upon mixing, the motors bind to the microtubule and release the mant-ADP, which results in a fall in fluorescence. Because at low microtubule concentrations mant-ADP release is rate limited by microtubule binding, a linear fit of the rates to the microtubule concentration yields the bimolecular on-rate.[16,43,48,49] Notably, swapping the K-loop out of KIF1A had little effect on the bimolecular on-rate of KIF1A, contrasting with its effect on the run length (Fig. 2D). However, swapping the KIF1A loop-12 into kinesin-1 caused a 5-fold increase in the on-rate (**Error! Reference source not found.**G).

Positive charge in the KIF1A K-loop enhances processivity by decreasing the rate of detachment from a vulnerable 1HB state

To investigate the mechanism by which the K-Loop enhances KIF1A processivity, we quantified key rate constants in the KIF1A chemomechanical cycle that determine motor run length. Previous work established that kinesin processivity is determined by a kinetic race as the motor takes a forward step, as follows.[18,19] Following ATP hydrolysis, kinesin is in a vulnerable one-head-bound state that can resolve either by the tethered head completing a forward step by binding to the next tubulin binding site and transitioning to a tight binding state, or by the motor dissociating from the

microtubule and terminating the run (**Error! Reference source not found.**A).[16,18] Thus, in principle the K-loop could enhance KIF1A processivity by some combination of increasing the on-rate that the tethered head binds to its next binding site (k_{on}^{TH}) and decreasing the rate that the bound head detaches from the microtubule (k_{detach}).

To test whether the K-loop affects the detachment rate of KIF1A from its weak-binding state, we used an affinity assay in conjunction with a microtubule on-rate measurement. The dissociation constant is defined as $K_D = \frac{k_{detach}}{k_{on}^{Mt}}$; thus, by measuring both K_D and k_{on}^{Mt} for each motor, we can calculate k_{detach}. To estimate the K_D of $1A_{393}$ and 1A-K1L12, we carried out a microtubule pelleting assay in 2 mM ADP to mimic the weak-binding post-hydrolysis state. In this assay, varying concentrations of microtubules are mixed together with a constant motor concentration, the mixture is pelleted, and the GFP fluorescence is used to determine the fraction of motors bound to the microtubule at each [Mt].[43] As shown in **Error! Reference source not found.**B, swapping out Loop-12 of KIF1A reduced the microtubule affinity in ADP by four-fold, with $K_D = 1.3 \pm 0.8$ μM for $1A_{393}$, and $K_D = 5.1 \pm 4.3$ μM for 1A-K1L12. To relate these affinities to the affinity of the motor when it is processively walking along the microtubule, we repeated these pelleting assays in ATP. For both constructs, their K_D in ATP was similar to that in ADP (for $1A_{393}$, $K_D = 1.7 \pm 1.0$ μM in ATP and for 1A-K1L12, $K_D = 7.2 \pm 5.1$ μM in ATP; Fig. 3B), consistent with both motors spending most of their hydrolysis cycle in a weakly-bound ADP-like state, in agreement with previous work.[16] To calculate the detachment rate from the weak-binding state, we used the K_D in ADP together with the k_{on}^{Mt} results from Fig. 2D, which were 10.6 ± 0.5 μM^{-1} s^{-1} for $1A_{393}$ and 9.1 ± 2.5 μM^{-1} s^{-1} for 1A-K1L12. From these values, we calculated k_{detach} in ADP to be 18 ± 11 s^{-1} for $1A_{393}$ and 66 ± 50 s^{-1} for 1A-K1L12, matching the 4-fold difference in the run lengths in Fig. 2B.

To more directly test whether the K-loop slows dissociation of KIF1A from the microtubule in the weakly-bound post-hydrolysis state, we used single-molecule TIRF microscopy to measure the dwell time of landing events in 2 mM ADP. For $1A_{393}$, the dwell time distribution was well fit by a single-exponential with a time constant of 1.8 ± 0.08 s (**Error! Reference source not found.**F), corresponding to an off-rate of 0.56 ± 0.02 s^{-1}. When we repeated the experiment for 1A-K1L12,

the kymographs showed a population of very transient events along with a population of longer duration events (Fig. S3). The dwell time distribution was well fit to a double exponential with a fast population of 0.03 ± 0.01 s (k_{off} = 33 s^{-1}) that constituted ~40% of the events, and a slow population of 0.3 ± 0.03 s (k_{off} = 3.3 s^{-1}) that constituted the other ~60 % of the events (Fig. 3C). Relative to the $1A_{393}$ dwell time of 1.8 s, these 1A-K1L12 dwell times correspond to a 60- and 6-fold faster off-rate when the K-loop of KIF1A is swapped out. Thus, both the microtubule pelleting assay and the single-molecule dwell time assay find that the apparent off-rate of KIF1A in the weakly-bound ADP state is increased when the K-loop is replaced by the equivalent sequence from kinesin-1.

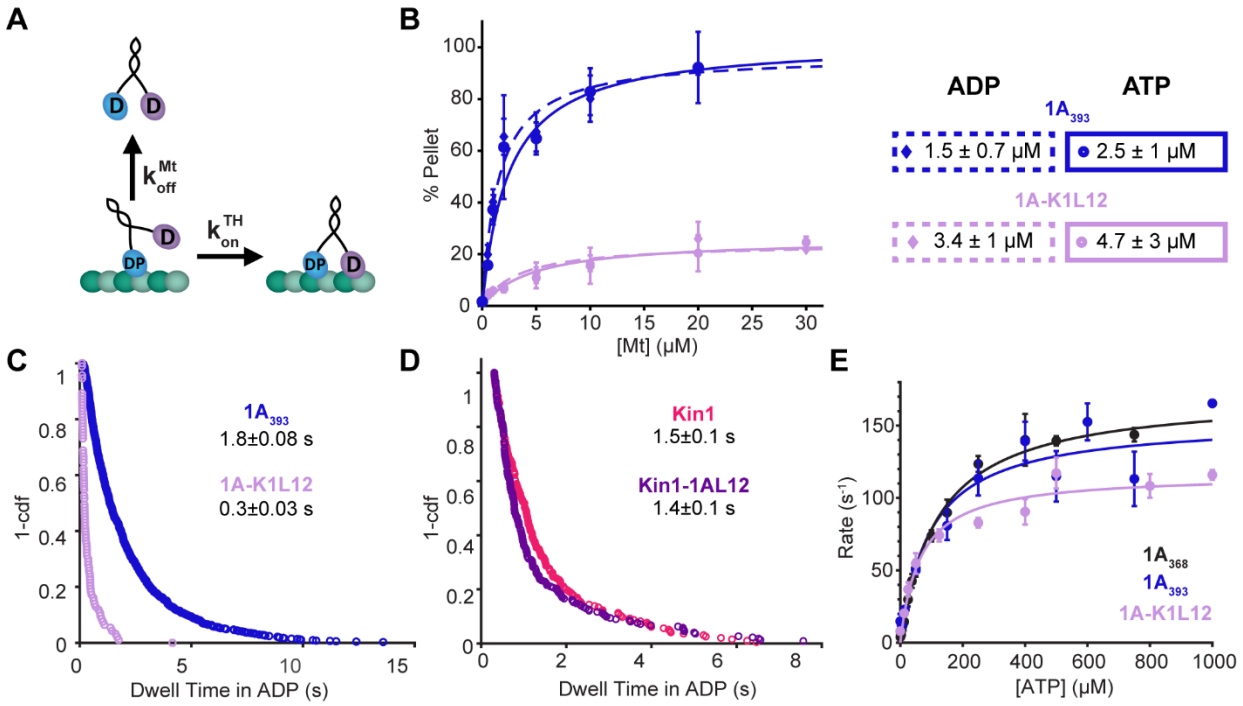

Figure 3: **K-Loop regulates KIF1A superprocessivity via detachment rate in the kinetic race A,** Diagram of transitions involved in the Kinetic Race. Tethered-head attachment rate k_{on}^{TH} and microtubule detachment rate k_{detach}. D, ADP; DP, ADP+Pi. **B,** Microtubule pelleting assay of $1A_{393}$ and 1A-K1L12 in 2 mM ADP or ATP and BRB80. Plot is the percent of GFP-labelled motors in the microtubule pellet after centrifugation as a function of microtubule concentration. To account for any inactive motors, data are normalized to the concentration of motors bound in 1 mM AMPPNP, which induces a strongly-bound state of the motor. Fits with a Langmuir binding isotherm give the K_D and maximal binding fraction for each condition. $1A_{393}$ gives a V_{max} of 97± 10 % and 102 ± 20 % in ADP and ATP, respectively. Despite the normalization to percent binding

in AMPPNP, 1A-K1L12 does not reach full binding in this microtubule range with a V_{max} of 24 ± 3 % and 26 ± 7 % in ADP and ATP, respectively. This could be because the K_D is actually around 30 μM or there is only ~50% maximal binding in ADP and ATP. Values are fit ± 95% CI and error bars are mean ± relative error. **C,** Dwell time distribution of 1A-K1L12 (light purple circles) in 2 mM ADP and BRB80. Biexponential fit gives dwell times of 0.03 ± 0.01 s and 0.3 ± 0.03 s (fit ± 95% confidence interval) with equal weights for the fast and slow populations. Data were collected at 50 frames per second. **D,** Dwell time distribution of Kin1 (pink circles) and K1-1AL12 (dark purple circles) in 2 mM ADP and BRB80. Single exponential fits give dwell times of 1.5 ± 0.1 s and 1.4 ± 0.1 s, respectively (fit ± 95% confidence interval). **E,** ATP-triggered Half-Site Release assay of $1A_{368}$ (black circles), $1A_{393}$ (blue circles), and 1A-K1L12 (light purple circles). Plot is the observed rate as a function of ATP concentration, and fitting with Michaelis-Menten equation give K_M and k_{max} values for each condition. For $1A_{368}$ (black circles), $1A_{393}$ (blue circles), and 1A-K1L12 (light purple circles), k_{max} were 172 ± 10, 154 ± 30, and 116 ± 13.4 s^{-1}, respectively; K_M were 119 ± 20, 96 ± 53, and 64 ± 28 μM, respectively (fit ± 95% confidence interval).

As described by the kinetic race shown in Fig. 3A, it is also possible that the K-loop contributes to KIF1A processivity by enhancing the rate that the tethered head attaches to the microtubule during a forward step, To test this possibility, we carried out an ATP-triggered Half-Site release assay, as follows (**Error! Reference source not found.**E). First, we incubated the motors with mant-ADP and microtubules to establish a complex of motors bound to the microtubule in a one-head-bound state, with mant-ADP trapped in the tethered-head. Then, we flushed this solution against varying concentrations of unlabeled ATP to initiate the binding of the tethered head and subsequent mant-ADP release. We next fit the fluorescent delay from the release of mant-ADP with an exponential function at each ATP concentration, plotted the observed rates versus the corresponding [ATP], and fit the data to a Michaelis-Menten curve. The observed rate constant at saturating ATP concentrations, k_{max}, represents ATP hydrolysis, tethered head binding, and the subsequent release of mant-ADP. Because hydrolysis and mant-ADP are thought to be fast,[16] it serves as a proxy for the tethered head binding rate. The k_{max} for our $1A_{393}$ construct (154 ± 30 s^{-1}; fit ± 95% confidence interval) was similar to $1A_{368}$ (172 ± 10 s^{-1}), indicating that the neck-coil does not alter the tethered head on-rate. For 1A-K1L12, k_{max} decreased slightly to 116 ± 13 s^{-1}, indicating that, in addition to slowing the microtubule off-rate, the K-loop may enhance KIF1A

superprocessivity by increasing the tethered head on-rate, k_{on}^{TH}. However, a caveat of this conclusion is that because the tethered-head attachment is thought to be the rate limiting step of the KIF1A chemomechanical cycle,[16] a decrease in this rate should also decrease the overall motor velocity. Instead, the velocity for 1A-K1L12 was 20% faster than the $1A_{393}$ (**Error! Reference source not found.**C). Additionally, the calculated k_{on}^{TH} for 1A-K1L12 of 116 ± 13 s^{-1} is slower than the overall stepping rate of 212 s^{-1} (calculated as 1.7 μm/s velocity ÷ 8 per step). Thus, the question of whether the K-loop enhances the tethered-head on-rate is inconclusive from this experiment.

As a second strategy for estimating the tethered head attachment rate, we calculated it based on the observed run length in ATP and the measured detachment rate in ADP, as follows. From on the kinetic race shown in Fig. 3A,[18] the probability of detaching during each cycle is:

$$p_{detach} = \frac{k_{detach}^{ADP}}{k_{on}^{TH} + k_{detach}^{ADP}} \approx \frac{k_{detach}^{ADP}}{k_{on}^{TH}} \qquad \text{Eq. 1}$$

The number of steps a motor takes before dissociating can be estimated as the inverse of the detachment probability:

$$RL_{steps} = \frac{1}{p_{detach}} \approx \frac{k_{on}^{TH}}{k_{detach}^{ADP}} \qquad \text{Eq. 2}$$

Thus, the tethered head attachment rate can be estimated by multiplying the measured detachment rate in ADP by the measured run length in ATP:

$$k_{on}^{TH} = k_{detach}^{ADP} * RL_{steps} \qquad \text{Eq. 3}$$

Table 1 shows the off-rates in ADP calculated from measured dwell times in Fig. 3 C and D, along with the run lengths calculated in number of steps from Fig. 2 B and E, and the resulting calculated tethered head attachment rate. The first result is that the calculated tethered head on-rates are roughly three-fold faster for KIF1A than kinesin-1. The key result from this analysis is that for KIF1A, swapping out the K-loop has no effect on the calculated tethered-head on-rate. In summary, the K-loop contributes to the superprocessivity of KIF1A by slowing the off-rate of the motor from the vulnerable 1HB state, and the K-loop does not modulate the processivity of KIF1A by enhancing the tethered head attachment rate.

Table 1: Calculations of Tethered-head attachment rate for different constructs.

Dwell times are fit ± 95% CI from Fig. 3 and off-rates are inverse of dwell times with propagated errors. Run Length (RL) in steps are the RL taken from Fig. 2 divided by the step size (8-nm), and errors are ± 95% CI. k_{on}^{TH} were calculated using Eq. 3, with errors propagated from off-rates and RL.

Construct	Dwell Time (s)	Off-rate (s^{-1})	RL in steps (RL/8 nm)	Calc. k_{on}^{TH} (s^{-1})
$1A_{393}$	1.8 ± 0.08	0.56 ± 0.02	375 ± 3	208 ± 8
1A-K1L12	0.3 ± 0.03	3.3 ± 0.3	63 ± 1	208 ± 19
Kin1	1.5 ± 0.1	0.67 ± 0.04	100 ± 3	67 ± 5
K1-1AL12	1.4 ± 0.1	0.71 ± 0.05	113 ± 3	80 ± 6

KIF1A run length scales with charge of the K-loop

In principle, swapping in the K-loop of kinesin-1 could be reducing the KIF1A run length either solely due to differences in positive charge, or through some combination of charge and the length of the loop. To test whether the run length data can be accounted for exclusively based on the charge of loop 12, we designed three additional loop-12 mutant constructs having the same length as wild-type but having varying net charge in the loop-12 domain. First, we increased the total charge of loop-12 in our KIF1A(1-393)-K560 construct by replacing three of the native uncharged residues with lysines, resulting in a net charge of +7 in loop-12; we refer to this construct as the Super-K-Loop (Fig. 4A). Using single molecule motility assays in BRB80 at 2 mM ATP, we found that the run length increased ~2-fold and the segmented velocity was slightly slower compared to the control (**Error! Reference source not found.** B-C; Table 2). We also used stopped-flow to measure the bimolecular on-rate, k_{on}^{Mt}, and found that the Super-K-Loop on-rate was 1.5-fold faster than wild-type, but the values were within fit error of one another (Fig. 4D).

Next, to test whether reducing the net charge of loop-12 reduces the run length, we replaced a portion of the of the lysine residues in loop-12 with glutamine. Glutamine was chosen because it is uncharged in our buffer (pH 6.9) and the side chain is of similar size to lysine, minimizing potential steric effects. We made constructs with four and five Lys-Glu substitutions (1A-4Q and 1A-5Q), resulting in net charges of -1 and 0 in Loop-12, respectively (Fig. 4A). In contrast to the K-loop swap, we found no processive events for 1A-5Q or 1A-4Q in BRB80 (Fig. H). However, both glutamine constructs were processive in BRB12 buffer, confirming that the lack of events in BRB80 was not due to protein misfolding or other effect on motor activity (see representative kymographs in Fig. S4).

We quantified the processivity of the loop-12 charge constructs in BRB12 buffer and found that the run lengths scaled with the charge of loop-12. Compared to wild-type $1A_{393}$ (14 ± 0.4 μm; Fig 4E), 1A-K1L12 with a net charge of +1 had a 2-fold shorter run length than the wild type (6.7 ± 0.1 μm), 1A-4Q with net neutral charge was ~5-fold shorter (2.6 ± 0.1 μm), and 1A 5Q with a net

charge -1 was ~10-fold shorter (1.2 ± 0.1 μm) (**Error! Reference source not found.**E and

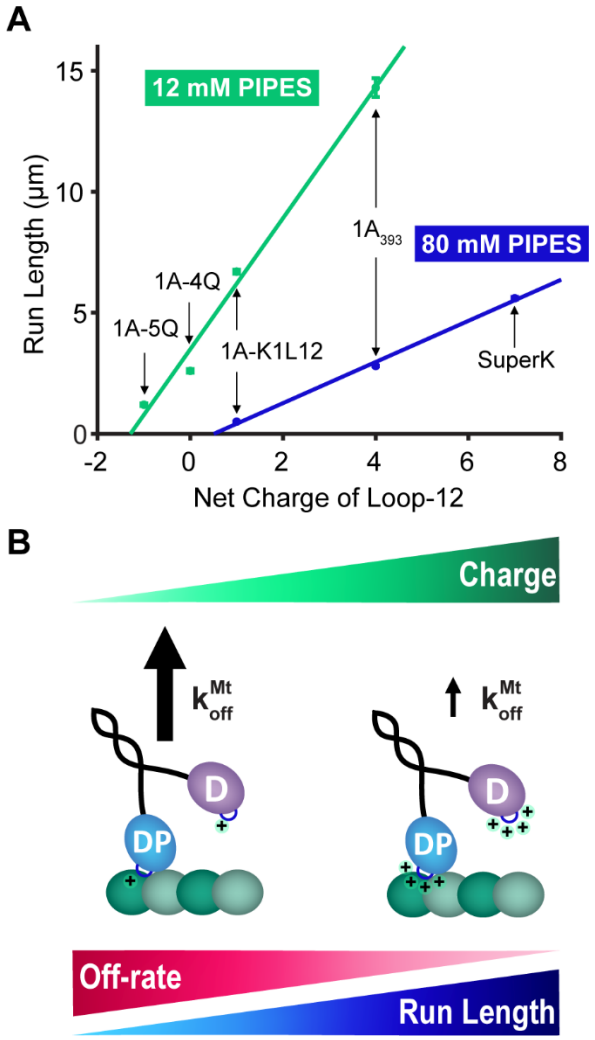

Figure 6; Table 3). The velocities in BRB12 also differed, but not in a charge-dependent manner: $1A_{393}$ was 1.1 ± 0.6 μm/s, 1A-K1L12 was faster at 1.6 ± 0.8 μm/s, 1A-4Q matched wild-type at 1.0 ± 0.6 μm/s, and 1A-5Q was slower at 0.6 ± 0.4 μm/s (Fig. 4F; Table 3). Interestingly the bimolecular on-rates in BRB12 buffer of the three mutants were similar to one another and they were all ~5-fold slower than $1A_{393}$ (Fig. 4G). Thus, the key feature of KIF1A loop-12 that enhances the motor's processivity is the positive charge rather than the longer length relative to kinesin-1.

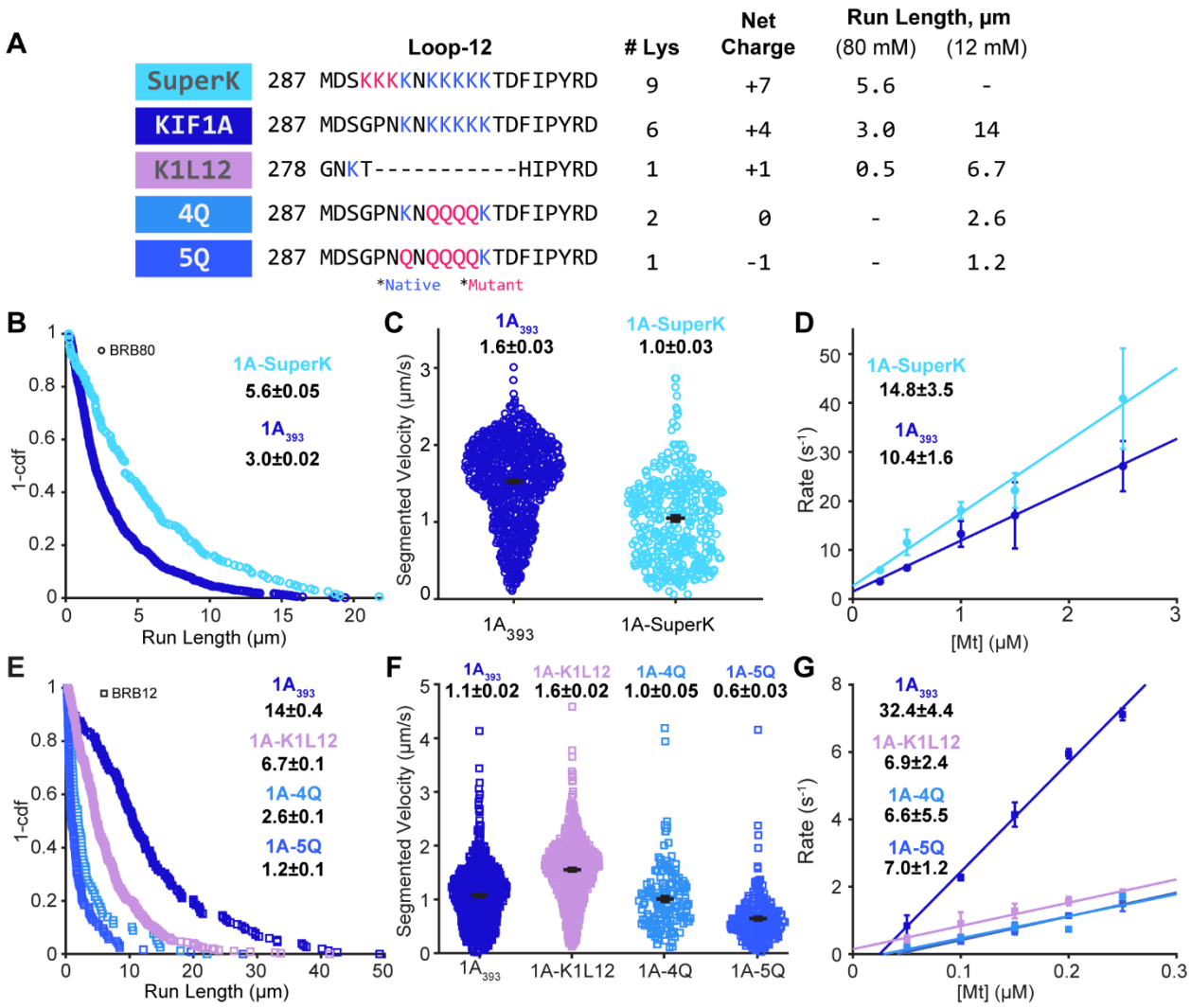

Figure 4: **Charge of the K-Loop regulates superprocessivity**

A, Sequence of the Loop-12 domain in the protein constructs used. Number of lysine residues and net charge of the domain are also given. Mutations are in red; native lysines are in green. Representative kymographs in Fig. S4. **B,** Run length distribution of $1A_{393}$ (blue circles) and 1A-SuperK (light blue circles) in BRB80 and 2 mM ATP. Single exponential fits give run lengths of 3.0 ± 0.02 and 5.6 ± 0.05 µm, respectively (fit ± 95% confidence interval). **C,** Velocity distribution of $1A_{393}$ (blue circles) and 1A-SuperK (light blue circles) in BRB80 and 2 mM ATP. Average velocities for segments with $\Delta x > 3$ pixels are 1.6 ± 003 and 1.0 ± 0.03 µm/s, respectively (mean ± SEM). **D,** Bimolecular on-rates of $1A_{393}$ (blue circles) and 1A-SuperK (light blue circles) in BRB80. Linear fits give k_{on}^{Mt} of 10.4 ± 1.6 and 14.8 ± 3.5 $\mu M^{-1}s^{-1}$, respectively (fit ± 95% confidence interval). Points are mean ± SEM. **E,** Run length distribution of $1A_{393}$ (blue squares),

1A-4Q (light blue squares), 1A-5Q (medium blue squares) and 1A-K1L12 (light purple squares) in BRB12 and 2 mM ATP. Single exponential fits give run lengths of 14 ± 0.4, 2.6 ± 0.1, 1.2 ± 0.1, and 6.7 ± 0.1 μm, respectively (fit ± 95% confidence interval). **F,** Velocity distribution of $1A_{393}$ (blue squares), 1A-K1L12 (light purple squares), 1A-4Q (light blue squares), and 1A-5Q (medium blue squares) in BRB12 and 2 mM ATP. Average velocities for segments with $\Delta x > 3$ pixels are 1.1 ± 0.02, 1.6 ± 0.02, 1.0 ± 0.05, and 0.6 ± 0.03 μm/s, respectively (mean ± SD). **G,** Bimolecular on-rates of $1A_{393}$ (blue squares), 1A-4Q (light blue squares), 1A-5Q (medium blue squares) and 1A-K1L12 (light purple squares) in BRB12. Linear fits give k_{on}^{Mt} of 32.4 ± 4.4, 6.6 ± 5.5, 7.0 ± 1.2 and 6.9 ± 2.4 $\mu M^{-1}s^{-1}$, respectively (fit ± 95% confidence interval). Points are mean ± SEM.

Human disease mutations adjacent to the K-loop impair KIF1A motility

To extend our understanding of the role of loop-12 in KIF1A motility, we investigated the motile properties of a set of patient derived mutations near the K-loop. In a library of KIF1A mutations in patients suffering from KIF1A neurological disorders (KAND), there are no mutations in the charged lysines in loop-12, but there are a number of mutations adjacent to loop-1. In the well conserved 'PYRD' sequence at the carboxy end of the loop, three pathogenic mutations have been identified in humans: R307P, R307Q, and P305L (**Error! Reference source not found.**A). Notably, these mutations changed either sequence or charge without altering the length of Loop-12 or any of the lysine residues within the 'K-loop' region.

We first examined R307P, R307Q, and P305L mutants using single molecule tracking in BRB80 and 2 mM ATP and observed no motility for any of these disease mutants (**Error! Reference source not found.**B). When the ionic strength was lowered using BRB12 buffer, 1A-R307P and 1A-R307Q showed a higher frequency of landing events and longer duration of diffusive events, but still no persistent directionality was detected (**Error! Reference source not found.**B). In contrast, 1A-P305L did show processive movement in BRB12. The 1A-P305L run length was ~5-fold shorter and the velocity was ~2-fold slower than $1A_{393}$ in BRB12 (**Error! Reference source not found.**C-D). It was previously proposed that the P305L mutation decreases the motor on-rate through a conformational change of the K-Loop.[50] Thus, it is possible that by lowering the ionic

strength, and therefore increasing the microtubule on-rate, the higher population of bound motors leads to a higher population of processive motors, allowing for visualization. To directly measure the on-rate of the motor to the microtubule, we used the stopped flow k_{on}^{Mt} assay in BRB12 (**Error! Reference source not found.**E). The 1A-P305L mutant had a ~3-fold lower on-rate than $1A_{393}$, supporting this hypothesis. Interestingly, the 1A-P305L on-rate of 9.3 ± 3 $\mu M^{-1}s^{-1}$ (Fig. 5E) was faster than either the loop swap mutant 1A-K1L12 (6.9 ± 2 $\mu M^{-1}s^{-1}$) or the two glutamine mutants (6.6 ± 5.5 $\mu M^{-1}s^{-1}$ for 1A-4Q and 7.0 ± 1 $\mu M^{-1}s^{-1}$ for 1A5Q) in BRB12 (Fig. 4G; Table 3).

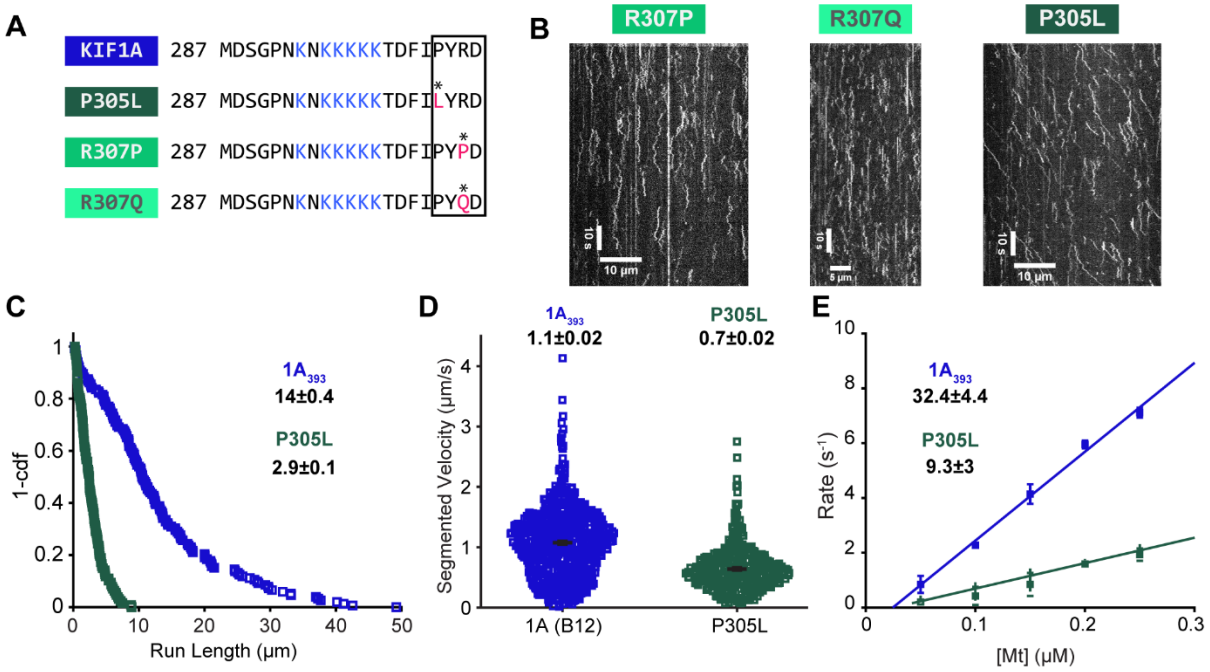

Figure 5: **Pathogenic mutations in Loop-12 hinder KIF1A motility**

A, Sequence of the Loop-12 for wild-type and mutants, with point mutations indicated in red and conserved distal region indicated by a box. **B,** Example kymographs of 1A-R307P, 1A-R307Q, and 1A-P305L in 2 mM ATP or BRB12 (as noted in figure). **C,** Run length distribution of $1A_{393}$ (blue squares) and 1A-P305L (green squares) in BRB12 and 2 mM ATP. Single exponential fits give run lengths of 14 ± 0.4 and 2.9 ± 0.1 µm, respectively (fit ± 95% confidence interval). **D,** Velocity distribution of $1A_{393}$ (blue squares) and 1A-P305L (green squares) in BRB12 and 2 mM ATP. Average velocities for segments with $\Delta x > 3$ pixels were 1.1 ± 0.02 and 0.7 ± 0.02 µm/s, respectively (mean ± SEM). **E,** Bimolecular on-rates of $1A_{393}$ (blue squares) and 1A-P305L (green squares) in BRB12. Linear fits give k_{on}^{Mt} of 32.4 ± 4.4 and 9.3 ± 3 $\mu M^{-1}s^{-1}$, respectively (fit ± 95% confidence interval). Points are mean ± SEM.

Table 2: Summary of Data in BRB80

Construct	RL (μm)	Vel (μm/s)	ADP Dwell (s)	k_{on}^{Mt} ($\mu M^{-1} s^{-1}$)
1A(1-393)	3.0 ± 0.02	1.6 ± 0.03 *	1.8 ± 0.08	10.6 ± 0.5
1A-K1L12	0.5 ± 0.004	1.7 ± 0.03	0.3 ± 0.03	9.1 ± 2.5
K1	0.8 ± 0.02	0.7 ± 0.01	1.5 ± 0.1	1.7 ± 0.6
K1-1AL12	0.9 ± 0.02	0.8 ± 0.01	1.4 ± 0.1	9.9 ± 2.9
Super-K	5.6 ± 0.05	1.0 ± 0.03 *	-	14.8 ± 3.5

*Segmented Velocity reported.

Table 3: Summary of Data in BRB12

Construct	RL (μm)	Vel (μm/s)	k_{on}^{Mt} ($\mu M^{-1} s^{-1}$)
1A(1-393)	14.3 ± 0.4	1.1 ± 0.02 *	32 ± 4.4
1A-K1L12	6.7 ± 0.1	1.6 ± 0.02 *	6.9 ± 2.4
4Q	2.6 ± 0.1	1.0 ± 0.05 *	6.6 ± 5.5
5Q	1.2 ± 0.1	0.6 ± 0.03 *	7.0 ± 1.2
P305L	2.9 ± 0.1	0.7 ± 0.02 *	9.3 ± 3

*Segmented Velocity reported.

Discussion

The positively charged loop-12 in kinesin-3 motors, known as the K-Loop, has been a topic of interest in the field for many years, but there has yet to be a consensus on the role of the K-loop in the mechanism of KIF1A superprocessivity. In this work, we have established a comprehensive understanding of the mechanism of the K-Loop in the KIF1A chemomechanical cycle. We conclude that the unique superprocessivity of KIF1A originates from the charge-dependent interaction of loop-12 with the microtubule, resulting in a reduction in off-rate from the post-hydrolysis one-head-bound (1HB) state (Fig. 6). This stabilization of the weak-binding state allows time for the tethered head to bind to the next binding site and complete the step, and thus maximizes the number of steps the motor takes before terminating a processive run.

Despite an appreciation of the importance of the K-loop, there are contradictions in the literature regarding the role of the K-loop in KIF1A superprocessivity. Early work made the striking finding

that KIF1A monomer constructs move processively through a combination of intermittent forward steps and 1D diffusion along the microtubule.[26,51] The microtubule affinity of these monomers was shown to depend on the negatively charged C-terminal tail of tubulin, scale with the amount of positive charge in loop-12, and to be enhanced in low salt buffers. Subsequently, it was shown that full-length KIF1A is dimeric and the motility of dimer constructs was fast, superprocessive, and lacked the diffusional behavior of the monomers.[31,52] However, using a KIF1A dimer truncated after the neck coil (1-393 aa), it was found that replacing the KIF1A loop-12 by that of kinesin-1 did not diminish the run length,[32] a result that was puzzling in light of the monomer results. Subsequent work showed that, unlike kinesin-1, the neck-coil domain of KIF1A is insufficient to stably dimerize the motor, however stabilized dimers can be created by adding a leucine zipper sequence downstream of the neck coil.[33] Experiments using stabilized dimers in BRB12 found that swapping out the KIF1A K-loop or reducing its charge by replacing three lysines by alanines led to a two- to five-fold decrease in processivity.[20,27,31] These results are consistent with our six-fold decrease in processivity following a loop-12 swap in BRB80. How can these studies be resolved? Upon closer inspection, the apparent lack of influence of loop-12 on KIF1A processivity can be explained by the fact that the construct used in that work (KIF1A(1-393)) lacked a distal coiled-coil region that is needed to stabilize the dimer.[32] In that work, KIF1A(1-393) had a run length of 2.6 µm, the loop-swap mutant had a run length of 3.6 µm, and the stably dimerized KIF1A(1-393)-LZ had a run length of 9.8 µm.[32,33] Thus, the apparent lack of influence of the K-loop in the truncated dimer lacking a stabilizing LZ domain can be explained by run lengths being terminated by the motor reverting to monomers and dissociating from the microtubule rather than termination of a processive run by normal dissociation of the dimer. As a competing process, this premature termination would mask any change in run length due to the loop swap.

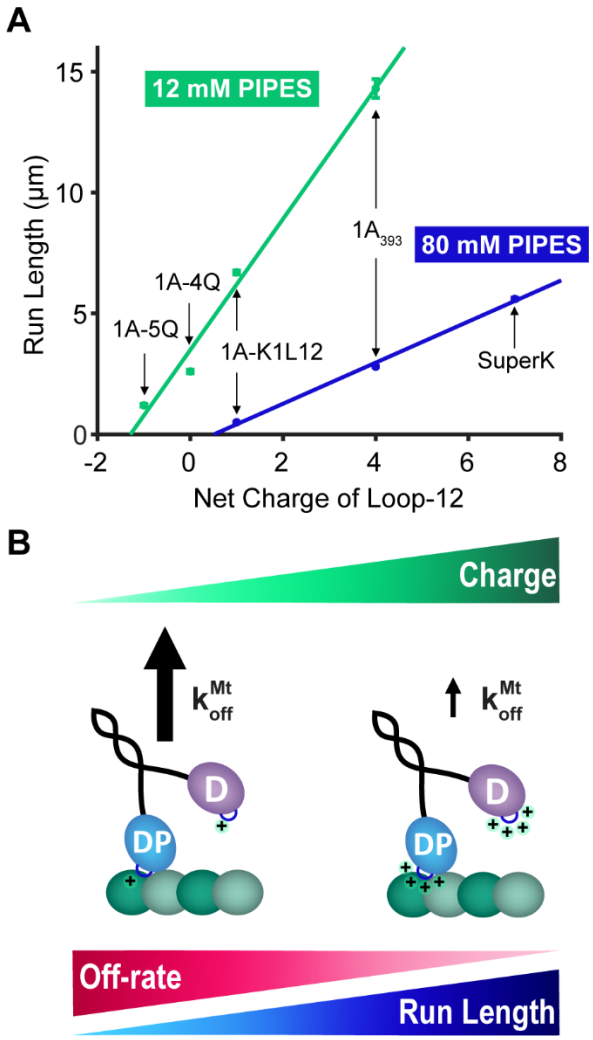

Figure 6: **Run Length of KIF1A is dependent on Charge of Loop-12**

A, Run Length of the various processive constructs used in this study, plotted as a function of the net charge of their Loop-12 domain, in BRB12 and BRB80. Points are from the 1-CDF plots in previous figures (fit ± 95% CI). Linear fits to the points in BRB12 and BRB80 give slopes of 2.7 ± 0.9 and 0.9 ± 0.6, respectively (fit ± 95% CI). **B,** Diagram depicting how increasing positive charge in Loop-12 leads to a slower off-rate in ADP that results in longer run lengths.

By measuring key transitions in the kinetic race that defines processivity, we find that the principal role of the K-loop is to stabilize the weak-binding, post-hydrolysis state of KIF1A. The finding from the pelleting assay that the K_D for microtubules is similar in ADP and ATP for both wild-type and Loop-12 swapped KIF1A emphasizes the importance of the weak binding state for KIF1A processivity. Their similar residence times are consistent with KIF1A spending the majority of its

cycle in a vulnerable one-head-bound ADP state, a key finding from a previous study.[16] The parallel reduction of the microtubule affinity in ADP and ATP upon swapping out the K-loop clearly demonstrates how decreasing the microtubule affinity in the ADP state dictates a reduction in run length. Because the other component of the kinetic race, tethered head attachment, also involves microtubule binding and hence might be expected to be modulated by charge in the K-loop, it was notable that swapping out the K-loop did not alter the tethered head on-rate. Tethered head binding involves both a mechanical component of the tethered head stretching to the next binding site, as well as a biochemical component of ADP release to achieve tight binding, and so the simplest interpretation of this result is that the rate tethered head binding is not substantially mediated by electrostatic interactions between the motor domain and the microtubule. Surprisingly, we found that swapping out the K-loop of KIF1A did not diminish the bimolecular on-rate in solution, meaning that electrostatics mediated by the K-loop do not play a strong role in the initial landing of KIF1A on the microtubule. This contrasts with kinesin-1, where inserting the K-loop of KIF1A did enhance the bimolecular on-rate in solution. This difference highlights the different kinetic tuning of the two motor families involved in the initial binding of the motor to the microtubule.

By systematically replacing lysines in KIF1A loop-12 with glutamines, we establish that it is the charge of loop-12, rather than its length that enhances KIF1A superprocessivity. Previous work with lysine substitutions produced mixed results. When all of the lysine residues were changed to alanines, the motor was non-processive, even in BRB12.[32] On the other hand, swapping out three lysines for alanines retained functionality but reduced the run length two-fold.[27] While our 1A-5Q and 1A-4Q mutants are incapable of processive movement in near physiological strength buffer, the finding that our 1A-5Q and 1A-4Q mutants are processive in BRB12 suggests that the nature of the side chains is important to the function of the loop. The importance of charge is highlighted by the finding that run lengths scaled linearly with the charge of loop-12 in both BRB80 and BRB12 (Fig. 6). The steeper slope in BRB12 is consistent with less charge shielding at low ionic strengths causing an enhanced electrostatic interaction that strongly contributes to the motor run length.

We also found that in near-physiological ionic strength buffer, swapping the KIF1A K-loop into kinesin-1 did not confer superprocessivity on this motor (**Error! Reference source not found.**). This result suggests that the KIF1A chemomechanical cycle is tuned such that it relies on the K-loop to achieve superprocessivity, whereas the kinesin-1 chemomechanical cycle is tuned to rely on different mechanisms to achieve processivity. Notably, inserting the KIF1A K-loop into kinesin-1 did not slow the detachment rate in the weak-binding ADP state (**Error! Reference source not found.**D), which explains why it did not enhance kinesin-1 processivity. Thus, binding of kinesin-1 in the ADP state is dominated by a different region of the microtubule binding domain, such as Loop-8 or Loop-11/α-4.[53] The lack of an effect on the run length suggests that inserting the K-loop into kinesin-1 also does not enhance the tethered head binding rate. This is notable because the bimolecular on-rate of kinesin-1 was enhanced by swapping in the K-loop, and it means that the bimolecular on-rate from solution is not predictive of the tethered-head binding rate.[20,22,32,40]

Interestingly, of the known KAND mutations, there are only recorded patient mutations at the highly conserved, distal end of Loop-12 and, to the best of our knowledge, none located within the K-loop itself (287-302 aa).[15] This suggests that the highly conserved distal region of loop-12 plays an important role, perhaps by interacting with the microtubule directly or indirectly through regulating the conformation of loop-12. We found that mutating R307 resulted in the motor being incapable of productive movement (**Error! Reference source not found.**), consistent with another recent study.[54] Published molecular dynamics simulations of motor-microtubule complexes found that R307 in KIF1A (and the equivalent R278 in kinesin-1) interact electrostatically with tubulin and thus likely contribute to the strength of microtubule binding.[53,55] Our results in BRB80 are consistent with this reduced affinity, but in BRB12 there were abundant diffusive interactions of both R307P and R307Q. One possibility is that this diffusive binding occurs solely through lysines in the K-loop, and the interaction of R307 with the microtubule occurs during the tight binding states in the stepping cycle. Interestingly, the calculated binding free energies of R307 with the microtubule in the strong-binding ATP and Apo states were similar to the weak-binding ADP state; thus, R307 does not appear to be involved in nucleotide-dependent differences that occur through the KIF1A nucleotide cycle. It is also notable that mutating R307 had a far more detrimental effect on the motor than replacing five out of six of the lysines in the K-loop. The other mutation we

investigated, P305L was found previously to strongly inhibit the microtubule on-rate of KIF1A, [50] and our stopped-flow results confirmed that result, while also finding that in BRB12 the run length and velocity were both diminished relative to wild-type.

The present study highlights different chemomechanical tuning strategies that kinesin-1 and kinesin-3 employ to carry out their intracellular transport functions. KIF1A is notable in being fast and superprocessive, and it does this by spending most of its hydrolysis cycle in a vulnerable one-head-bound state that is stabilized by electrostatic interactions between the K-loop and the microtubule. Importantly, this strategy causes the motor to detach readily under load, which is seemingly not an advantageous property for a transport motor.[20,21,23,56] However, KIF1A binds to the microtubule from solution at a much faster rate than kinesin-1, which may partly compensate for this detachment.[16] In contrast, kinesin-1 is able to walk processively against substantial loads,[21,56] but it walks more slowly, it binds to the microtubule out of solution more slowly, and in the absence of load has a considerably shorter run length.[16,32] As the mechanistic features of these motors become clarified, the next step is to understand how these functional properties scale up to multimotor cargo transport on diverse microtubules and bidirectional tug-of-war transport with dynein. Similarly, to understand how specific mutations lead to KAND disease states, it will be necessary to define the effect of other mutations on KIF1A chemomechanics and to extrapolate how those changes affect neuronal function.

Methods

Protein Preparation

Plasmids were designed in SnapGene and mutants were generated via Gibson assembly (Gibson Assembly® Cloning Kit from New England Biolabs)[57,58] or via QuickChange (Q5® Site-Directed Mutagenesis Kit from New England Biolabs).[59] Recombinant expression of motors in *E. coli* and purification via Ni-NTA chromatography were performed as described previously.[16]

Single Molecule Fluorescence Tracking

Single Molecule TIRF microscopy assays were performed as previously described.[16,41,43] Flow cells were injected sequentially with casein for surface blocking, rigor motors for binding microtubules to the surface,[37] and taxol-stabilized microtubules in BRB80 (80 mM PIPES, 1 mM EGTA, 1 mM $MgCl_2$, pH 6.9). The imaging buffer mixture was BRB80 with 20 mM D-glucose, 0.02 mg/ml glucose oxidase, 0.008 mg/ml catalase, and 10 mM DTT (dithiothreitol). Motors were diluted in imaging buffer with 0.5 mg/ml casein and 2 mM ADP/ATP (and equal molar $MgCl_2$). Videos were recorded at 10 frames per second in most cases, except 20 or 50 fps in ADP and BRB80 and 5 fps in ADP or ATP and BRB12. Kymograph analysis was carried out manually with ImageJ. Fits to the data distributions were done using MATLAB R2020b (MathWorks). Statistical analysis was carried out using GraphPad Prism7 t-test function (Kolmogorov-Smirnov test) to determine significance relative to the control.

Stopped Flow Assays

Stopped Flow assays, including k_{on}^{Mt} and ATP-triggered Half-Site Release were performed as previously described.[16] Concentrations mentioned below refer to the 'syringe concentrations' and the final concentrations in the chamber were half. The k_{on}^{Mt} assays in BRB80 were performed by flushing 300 nM of active motor dimers in 0.5 μM mant-ADP against 2 mM Mg-ADP and varying concentrations of taxol-stabilized microtubules (0.5 - 5 μM). In BRB12, 300 nM of active motor dimers in 5 μM mant-ADP were flushed against 2 mM Mg-ATP and varying concentrations of taxol-stabilized microtubules (0.1 – 0.5 μM). The ATP-triggered Half-Site Release assays were performed by incubating 0.5 μM active motor dimers with 6 μM of taxol-stabilized microtubules and 1 μM of excess mant-ADP to form a one-head-bound complex in solution. This complex was then flushed against varied concentrations of Mg-ATP.

Microtubule Pelleting Assays

In microtubule pelleting assays, GFP-labeled motors were incubated with varying concentrations of taxol-stabilized microtubules with 2 mM ADP or ATP. After a 5 minute incubation at room temperature, the solutions were spun down using an Airfuge at 30 psi for 10 minutes. A Molecular Devices FlexStation 3 Multimode Microplate Reader was used to measure the GFP concentration of the pellet and supernatant. Reported values (% pellet) were calculated as the fluorescence of the pellet divided by the sum of the pellet and supernatant. All values were normalized to a control value of motors in 2 mM AMPPNP and 20 μM taxol-stabilized microtubules.

References

(1) Hirokawa, N.; Noda, Y. Intracellular Transport and Kinesin Superfamily Proteins, KIFs: Structure, Function, and Dynamics. *Physiological Reviews* **2008**, *88* (3), 1089–1118.

(2) Miki, H.; Setou, M.; Kaneshiro, K.; Hirokawa, N. All Kinesin Superfamily Protein, KIF, Genes in Mouse and Human. *Proceedings of the National Academy of Sciences* **2001**, *98* (13), 7004–7011.

(3) Hirokawa, N.; Noda, Y.; Tanaka, Y.; Niwa, S. Kinesin Superfamily Motor Proteins and Intracellular Transport. *Nature Reviews Molecular Cell Biology* **2009**, *10*, 682–696.

(4) Niwa, S.; Lipton, D. M.; Morikawa, M.; Zhao, C.; Hirokawa, N.; Lu, H.; Shen, K.; Niwa, S.; Lipton, D. M.; Morikawa, M.; Zhao, C.; Hirokawa, N.; Lu, H.; Shen, K. Autoinhibition of a Neuronal Kinesin UNC-104/KIF1A Regulates the Size and Density of Synapses. *CellReports* **2016**, *16* (8), 2129–2141.

(5) Yonekawa, Y.; Harada, A.; Okada, Y.; Funakoshi, T.; Kanai, Y.; Takei, Y.; Terada, S.; Noda, T.; Hirokawa, N. Defect in Synaptic Vesicle Precursor Transport and Neuronal Cell Death in KIF1A Motor Protein–Deficient Mice. *Journal of Cell Biology* **1998**, *141* (2), 431–441.

(6) Vecchia, S. della; Tessa, A.; Dosi, C.; Baldacci, J.; Pasquariello, R.; Antenora, A.; Astrea, G.; Bassi, M. T.; Battini, R.; Casali, C.; Cioffi, E.; Conti, G.; de Michele, G.; Ferrari, A. R.; Filla, A.; Fiorillo, C.; Fusco, C.; Gallone, S.; Germiniasi, C.; Guerrini, R.; Haggiag, S.; Lopergolo, D.; Martinuzzi, A.; Melani, F.; Mignarri, A.; Panzeri, E.; Pini, A.; Pinto, A. M.; Pochiero, F.; Primiano, G.; Procopio, E.; Renieri, A.; Romaniello, R.; Sancricca, C.; Servidei, S.; Spagnoli, C.; Ticci, C.; Rubegni, A.; Santorelli, F. M. Monoallelic KIF1A-Related Disorders: A Multicenter Cross Sectional Study and Systematic Literature Review. *Journal of Neurology* **2022**, *269* (1), 437–450.

(7) Nemani, T.; Steel, D.; Kaliakatsos, M.; DeVile, C.; Ververi, A.; Scott, R.; Getov, S.; Sudhakar, S.; Male, A.; Mankad, K.; Muntoni, F.; Reilly, M. M.; Kurian, M. A.; Carr, L.; Munot, P. KIF1A-Related Disorders in Children: A Wide Spectrum of Central

and Peripheral Nervous System Involvement. *Journal of the Peripheral Nervous System* **2020**, *25* (2), 117–124.

(8) Boyle, L.; Rao, L.; Kaur, S.; Fan, X.; Mebane, C.; Hamm, L.; Thornton, A.; Ahrendsen, J. T.; Anderson, M. P.; Christodoulou, J.; Gennerich, A.; Shen, Y.; Chung, W. K. Genotype and Defects in Microtubule-Based Motility Correlate with Clinical Severity in KIF1A-Associated Neurological Disorder. *Human Genetics and Genomics Advances* **2021**, *2* (2), 100026.

(9) Niwa, S. De Novo Mutations in KIF1A-Associated Neuronal Disorder (KAND) Dominant-Negatively Inhibit Motor Activity and Axonal Transport of Synaptic Vesicle Precursors. **2022**.

(10) Esmaeeli Nieh, S.; Madou, M. R. Z. Z.; Sirajuddin, M.; Fregeau, B.; McKnight, D.; Lexa, K.; Strober, J.; Spaeth, C.; Hallinan, B. E.; Smaoui, N.; Pappas, J. G.; Burrow, T. A.; McDonald, M. T.; Latibashvili, M.; Leshinsky-Silver, E.; Lev, D.; Blumkin, L.; Vale, R. D.; Barkovich, A. J.; Sherr, E. H. De Novo Mutations in KIF1A Cause Progressive Encephalopathy and Brain Atrophy. *Annals of Clinical and Translational Neurology* **2015**, *2* (6), 623–635.

(11) Pennings, M.; Schouten, M. I.; van Gaalen, J.; Meijer, R. P. P. P.; de Bot, S. T.; Kriek, M.; Saris, C. G. J. J.; van den Berg, L. H.; van Es, M. A.; Zuidgeest, D. M. H. H.; Elting, M. W.; van de Kamp, J. M.; van Spaendonck-Zwarts, K. Y.; Die-Smulders, C. de; Brilstra, E. H.; Verschuuren, C. C.; de Vries, B. B. A. A.; Bruijn, J.; Sofou, K.; Duijkers, F. A.; Jaeger, B.; Schieving, J. H.; van de Warrenburg, B. P.; Kamsteeg, E.-J. KIF1A Variants Are a Frequent Cause of Autosomal Dominant Hereditary Spastic Paraplegia. *European Journal of Human Genetics* **2020**, *28* (1), 40–49.

(12) Ohba, C.; Haginoya, K.; Osaka, H.; Kubota, K.; Ishiyama, A.; Hiraide, T.; Komaki, H.; Sasaki, M.; Miyatake, S.; Nakashima, M.; Tsurusaki, Y.; Miyake, N.; Tanaka, F.; Saitsu, H.; Matsumoto, N. De Novo KIF1A Mutations Cause Intellectual Deficit, Cerebellar Atrophy, Lower Limb Spasticity and Visual Disturbance. *Journal of Human Genetics* **2015**, *60* (12), 739–742.

(13) Krenn, M.; Zulehner, G.; Hotzy, C.; Rath, J.; Stogmann, E.; Wagner, M.; Haack, T. B.; Strom, T. M.; Zimprich, A.; Zimprich, F. Hereditary Spastic Paraplegia Caused

by Compound Heterozygous Mutations Outside the Motor Domain of the KIF1A Gene. *European Journal of Neurology* **2017**, *24* (5), 741–747.

(14) Hotchkiss, L.; Donkervoort, S.; Leach, M. E.; Mohassel, P.; Bharucha-Goebel, D. X.; Bradley, N.; Nguyen, D.; Hu, Y.; Gurgel-Giannetti, J.; Bönnemann, C. G. Novel de Novo Mutations in KIF1A as a Cause of Hereditary Spastic Paraplegia with Progressive Central Nervous System Involvement. *Journal of Child Neurology* **2016**, *31* (9), 1114–1119.

(15) Boyle, L.; Rao, L.; Kaur, S.; Fan, X.; Mebane, C.; Hamm, L.; Thornton, A.; Ahrendsen, J. T.; Anderson, M. P.; Christodoulou, J.; Gennerich, A.; Shen, Y.; Chung, W. K. Genotype and Defects in Microtubule-Based Motility Correlate with Clinical Severity in KIF1A-Associated Neurological Disorder. *Human Genetics and Genomics Advances* **2021**, *2* (2), 100026.

(16) Zaniewski, T. M.; Gicking, A. M.; Fricks, J.; Hancock, W. O. A Kinetic Dissection of the Fast and Superprocessive Kinesin-3 KIF1A Reveals a Predominant One-Head-Bound State during Its Chemomechanical Cycle. *Journal of Biological Chemistry* **2020**, *295* (52), 17889–17903.

(17) Taylor, E. W.; Borisy, G. G. Kinesin Processivity. *Journal of Cell Biology* **2000**, *151* (5), 1998–2000.

(18) Mickolajczyk, K. J.; Hancock, W. O. Kinesin Processivity Is Determined by a Kinetic Race from a Vulnerable One-Head-Bound State. *Biophysical Journal* **2017**, *112* (12), 2615–2623.

(19) Hancock, W. O.; Howard, J. Kinesin's Processivity Results from Mechanical and Chemical Coordination between the ATP Hydrolysis Cycles of the Two Motor Domains. *Proc Natl Acad Sci U S A* **1999**, *96* (23), 13147–13152.

(20) Arpağ, G.; Norris, S. R.; Mousavi, S. I.; Soppina, V.; Verhey, K. J.; Hancock, W. O.; Tüzel, E. Motor Dynamics Underlying Cargo Transport by Pairs of Kinesin-1 and Kinesin-3 Motors. *Biophysical Journal* **2019**, *116* (6), 1115–1126.

(21) Pyrpassopoulosa, S.; Gicking, A. M.; Zaniewski, T. M.; Hancock, W. O.; Ostapa, E. M. KIF1A Is Kinetically Tuned to Be a Super-Engaging Motor under Hindering Loads. *bioRxiv* **2022**, 1–45.

(22) Budaitis, B. G.; Jariwala, S.; Rao, L.; Yue, Y.; Sept, D.; Verhey, K. J.; Gennerich, A.; Kristen, J. Pathogenic Mutations in the Kinesin-3 Motor KIF1A Diminish Force Generation and Movement Through Allosteric Mechanisms. *bioRxiv* **2020**, *220* (4).

(23) Arpağ, G.; Shastry, S.; Hancock, W. O.; Tüzel, E. Transport by Populations of Fast and Slow Kinesins Uncovers Novel Family-Dependent Motor Characteristics Important for In Vivo Function. *Biophysical Journal* **2014**, *107* (8), 1896–1904.

(24) Okada, Y.; Hirokawa, N. A Processive Single-Headed Motor: Kinesin Superfamily Protein KIF1A. *Science (1979)* **1999**, *283* (5405), 1152–1157.

(25) Okada, Y.; Higuchi, H.; Hirokawa, N. Processivity of the Single-Headed Kinesin KIF1A through Binding to Tubulin. *Nature* **2003**, *424* (6948), 574–577.

(26) Okada, Y.; Hirokawa, N. Mechanism of the Single-Headed Processivity: Diffusional Anchoring between the K-Loop of Kinesin and the C Terminus of Tubulin. *Proceedings of the National Academy of Sciences* **2000**, *97* (2), 640–645.

(27) Lessard, D. v.; Zinder, O. J.; Hotta, T.; Verhey, K. J.; Ohi, R.; Berger, C. L. Polyglutamylation of Tubulin's C-Terminal Tail Controls Pausing and Motility of Kinesin-3 Family Member KIF1A. *Journal of Biological Chemistry* **2019**, *294* (16), 6353–6363.

(28) Nitta, R.; Kikkawa, M.; Okada, Y.; Hirokawa, N. KIF1A Alternately Uses Two Loops to Bind Microtubules. *Science (1979)* **2004**, *305* (5684), 678–683.

(29) Janke, C.; Magiera, M. M. The Tubulin Code and Its Role in Controlling Microtubule Properties and Functions. *Nature Reviews Molecular Cell Biology* **2020**, *21* (6), 307–326.

(30) Roll-Mecak, A. The Tubulin Code in Microtubule Dynamics and Information Encoding. *Developmental Cell* **2020**, *54* (1), 7–20.

(31) Tomishige, M.; Klopfenstein, D. R.; Vale, R. D.; Michio Tomishige; Dieter Klopfenstein; Ronald Vale; Tomishige, M.; Klopfenstein, D. R.; Vale, R. D.; Michio Tomishige; Dieter Klopfenstein; Ronald Vale. Conversion of Unc104/KIF1A Kinesin into a Processive Motor After Dimerization. *Science (1979)* **2002**, *297* (September), 2263–2267.

(32) Soppina, V.; Verhey, K. J. The Family-Specific K-Loop Influences the Microtubule on-Rate but Not the Superprocessivity of Kinesin-3 Motors. *Molecular Biology of the Cell* **2014**, *25* (14), 2161–2170.

(33) Soppina, V.; Norris, S. R.; Dizaji, A. S.; Kortus, M.; Veatch, S.; Peckham, M.; Verhey, K. J. Dimerization of Mammalian Kinesin-3 Motors Results in Superprocessive Motion. *PNAS* **2014**, *111* (15), 5562–5567.

(34) Ren, J.; Wang, S.; Chen, H.; Wang, W.; Huo, L.; Feng, W. Coiled-Coil 1-Mediated Fastening of the Neck and Motor Domains for Kinesin-3 Autoinhibition. *Proceedings of the National Academy of Sciences* **2018**, *115* (51), E11933–E11942.

(35) Ren, J.; Zhang, Y.; Wang, S.; Huo, L.; Lou, J.; Feng, W. Structural Delineation of the Neck Linker of Kinesin-3 for Processive Movement. *Journal of Molecular Biology* **2018**, *430* (14), 2030–2041.

(36) Feng, Q.; Mickolajczyk, K. J.; Chen, G.-Y.; Hancock, W. O. Motor Reattachment Kinetics Play a Dominant Role in Multimotor-Driven Cargo Transport. *Biophysical Journal* **2018**, *114* (2), 400–409.

(37) Mickolajczyk, K. J.; Deffenbaugh, N. C.; Ortega Arroyo, J.; Andrecka, J.; Kukura, P.; Hancock, W. O. Kinetics of Nucleotide-Dependent Structural Transitions in the Kinesin-1 Hydrolysis Cycle. *Proceedings of the National Academy of Sciences* **2015**, *112* (52), E7186–E7193.

(38) Huang, T.-G.; Suhan, J.; Hackney, D. D. Drosophila Kinesin Motor Domain Extending to Amino Acid Position 392 Is Dimeric When Expressed in Escherichia Coli. *J Biol Chem* **1994**, *269* (23), 16502–16507.

(39) Thorn, K. S.; Ubersax, J. A.; Vale, R. D. Engineering the Processive Run Length of the Kinesin Motor. *Journal of Cell Biology* **2000**, *151* (5), 1093–1100.

(40) Hughes, J.; Hancock, W. O.; Fricks, J. Kinesins with Extended Neck Linkers: A Chemomechanical Model for Variable-Length Stepping. *Bulletin of Mathematical Biology* **2012**, *74* (5), 1066–1097.

(41) Shastry, S.; Hancock, W. O. Neck Linker Length Determines the Degree of Processivity in Kinesin-1 and Kinesin-2 Motors. *Current Biology* **2010**, *20* (10), 939–943.

(42) Shastry, S.; Hancock, W. O. Interhead Tension Determines Processivity across Diverse N-Terminal Kinesins. *Proceedings of the National Academy of Sciences* **2011**, *108* (39), 16253–16258.

(43) Chen, G.-Y.; Arginteanu, D. F. J.; Hancock, W. O. Processivity of the Kinesin-2 KIF3A Results from Rear Head Gating and Not Front Head Gating. *Journal of Biological Chemistry* **2015**, *290* (16), 10274–10294.

(44) Hariharan, V.; Hancock, W. O. Insights into the Mechanical Properties of the Kinesin Neck Linker Domain from Sequence Analysis and Molecular Dynamics Simulations. *Cell Mol Bioeng* **2009**, *2* (2), 177–189.

(45) Kozielski, F.; Sack, S.; Marx, A.; Thorma, M. The Crystal Structure of Dimeric Kinesin and Implications for Microtubule-Dependent Motility. **1997**, *91*, 985–994.

(46) Mouat, M. F.; Manchester, K. L. The Intracellular Ionic Strength of Red Cells and the Influence of Complex Formation. *Comparative Haematology International* **1998**, *8* (1), 58–60.

(47) Dill, K. A.; Bromberg, S.; Stigter, D. *Molecular Driving Forces: Statistical Thermodynamics in Biology, Chemistry, Physics, and Nanoscience*; Garland Science, 2010.

(48) Cheng, J. Q.; Jiang, W.; Hackney, D. D. Interaction of Mant-Adenosine Nucleotides and Magnesium with Kinesin. *Biochemistry* **1998**, *37* (15), 5288–5295.

(49) Hackney, D. D.; Malik, A. S.; Wright, K. W. Nucleotide-Free Kinesin Hydrolyzes ATP with Burst Kinetics. *J Biol Chem* **1989**, *264* (27), 15943–15948.

(50) Lam, A. J.; Rao, L.; Anazawa, Y.; Okada, K.; Chiba, K.; Dacy, M.; Niwa, S.; Gennerich, A.; Nowakowski, D. W.; McKenney, R. J. A Highly Conserved 310 Helix within the Kinesin Motor Domain Is Critical for Kinesin Function and Human Health. *Science Advances* **2021**, *7* (18), 1–15.

(51) Hirokawa, N. Kinesin and Dynein Superfamily Proteins and the Mechanism of Organelle Transport. *Science (1979)* **1998**, *279* (5350), 519–526.

(52) Rashid, D. J.; Bononi, J.; Tripet, B. P. P.; Hodges, R. S. S.; Pierce, D. W. W.; Rashid, D. J.; Bononi, J.; Tripet, B. P. P.; Hodges, R. S. S.; Pierce, D. W. W.; Rashid, D. J.; Bononi, J.; Tripet, B. P. P.; Hodges, R. S. S.; Pierce, D. W. W. Monomeric and

Dimeric States Exhibited by the Kinesin-Related Motor Protein KIF1A. *Journal of Peptide Research* **2005**, *65* (6), 538–549.

(53) Scarabelli, G.; Soppina, V.; Yao, X. Q.; Atherton, J.; Moores, C. A.; Verhey, K. J.; Grant, B. J. Mapping the Processivity Determinants of the Kinesin-3 Motor Domain. *Biophysical Journal* **2015**, *109* (8), 1537–1540.

(54) Chiba, K.; Takahashi, H.; Chen, M.; Obinata, H.; Arai, S.; Hashimoto, K.; Oda, T.; McKenney, R. J.; Niwa, S.; Kyoko Chiba; Chen Min. Disease-Associated Mutations Hyperactivate KIF1A Motility and Anterograde Axonal Transport of Synaptic Vesicle Precursors. *Proceedings of the National Academy of Sciences* **2019**, *116* (37), 18429–18434.

(55) Grant, B. J.; Gheorghe, D. M.; Zheng, W.; Alonso, M.; Huber, G.; Dlugosz, M.; McCammon, J. A.; Cross, R. A. Electrostatically Biased Binding of Kinesin to Microtubules. *PLoS Biology* **2011**, *9* (11), 1001207.

(56) Budaitis, B. G.; Jariwala, S.; Rao, L.; Yue, Y.; Sept, D.; Verhey, K. J.; Gennerich, A.; Kristen, J.; Yue, Y.; Sept, D.; Verhey, K. J.; Gennerich, A. Pathogenic Mutations in the Kinesin-3 Motor KIF1A Diminish Force Generation and Movement Through Allosteric Mechanisms. *bioRxiv* **2020**, *220* (4).

(57) Gibson, D. G.; Glass, J. I.; Lartigue, C.; Noskov, V. N.; Chuang, R. Y.; Algire, M. A.; Benders, G. A.; Montague, M. G.; Ma, L.; Moodie, M. M.; Merryman, C.; Vashee, S.; Krishnakumar, R.; Assad-Garcia, N.; Andrews-Pfannkoch, C.; Denisova, E. A.; Young, L.; Qi, Z. N.; Segall-Shapiro, T. H.; Calvey, C. H.; Parmar, P. P.; Hutchison, C. A.; Smith, H. O.; Venter, J. C. Creation of a Bacterial Cell Controlled by a Chemically Synthesized Genome. *Science (1979)* **2010**, *329* (5987), 52–56.

(58) Gibson, D. G.; Young, L.; Chuang, R. Y.; Venter, J. C.; Hutchison, C. A.; Smith, H. O. Enzymatic Assembly of DNA Molecules up to Several Hundred Kilobases. *Nature Methods* **2009**, *6* (5), 343–345.

(59) Papworth, C.; Bauer, J. C.; Braman, J.; Wright, D. A. Site-Directed Mutagenesis in One Day with >80% Efficiency. *Strategies* **1996**, *9* (3), 3–4.

Supplemental Information

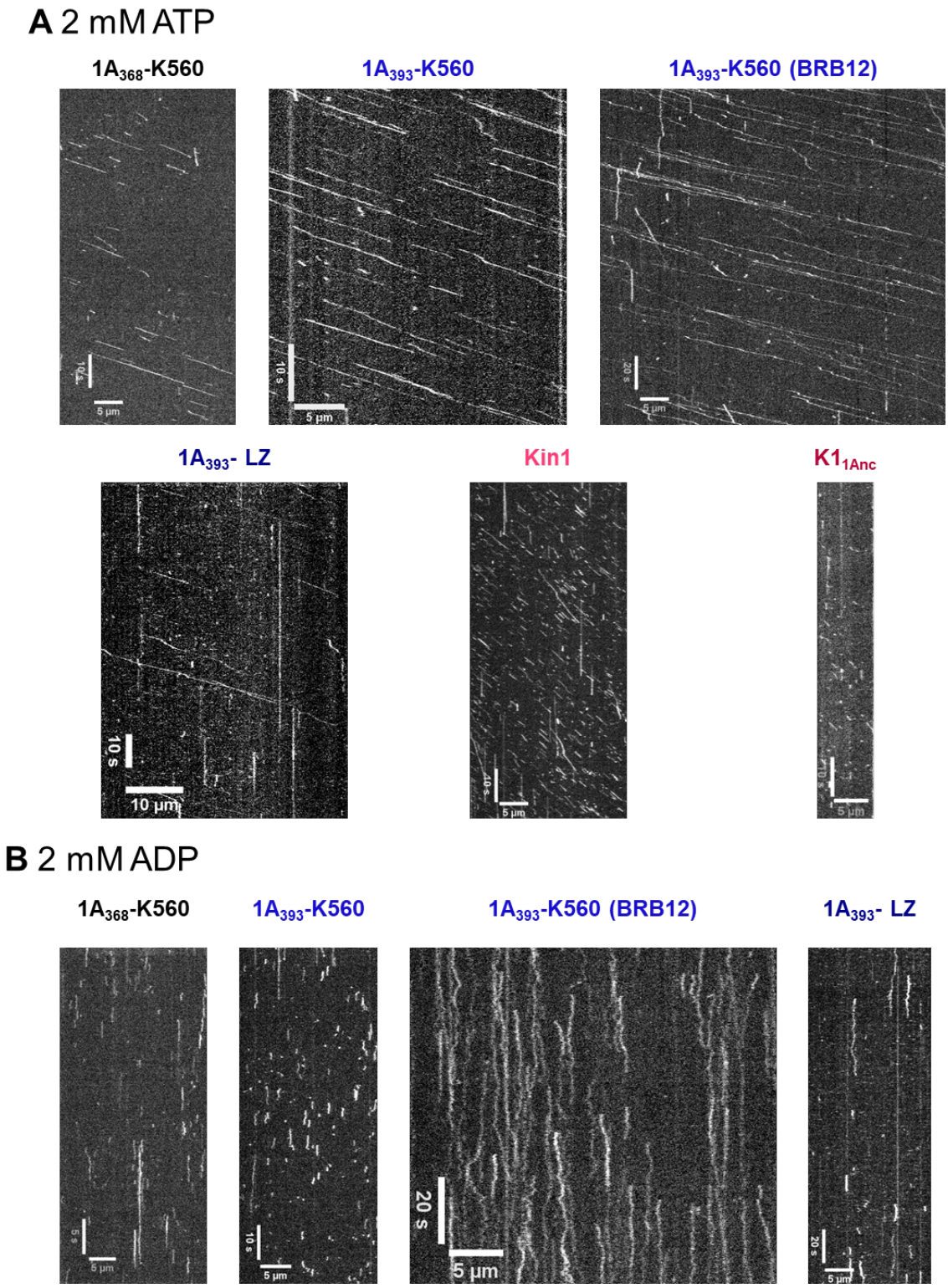

Figure S1: Example kymographs for different KIF1A and Kin1 constructs in ATP and ADP.

A, Kymograph of each construct in 2 mM ATP and BRB80 (unless otherwise noted). **B,** Kymograph of each construct in 2 mM ADP and BRB80 (unless otherwise noted).

	Domain	Sequence	Total Charges	Net Charge at pH 6.9	pI
Dimerization Domains	**LZ**	VKQLEDKVEELASKNYHLENEVARLKKLVG	(+7, -6)	+ 0.2	7.2
	LZ + Linker	GAGVKQLEDKVEELASKNYHLENEVARLKKLV GVPRAMLVPRGPVHRLGDPPVAT	(+11, -7)	+ 2.5	9.3
	K560 (345-560)	AEEWKRRYEKEKEKNARLKGKVEKLEIELARW RAGETVKAEEQINMEDLMEASTPNLEVEAAQT AAAEAALAAQRTALANMSASVAVNEQARLATE CERLYQQLDDKDEEINQQSQYAEQLKEQVMEQ EELIANARREYETLQSEMARIQQENESAKEEV KEVLQALEELTVNYDQKSQEIDNKNKDIDALN EELQQKQSVFNAASTELQQLKDMS	(+28, -49)	- 21	4.5
	KIF1A CC1 (394-523)	MTNALVGMSPSSSLSALSSRAASVSSLHERIL FAPGSEEAIERLKETEKIIAELNETWEEKLRR TEAIRMEREALLAEMGVAMREDGGTLGVFSPK KTPHLVNLNEDPLMSECLLYYIKDGVTRVGRE DA	(+16, -22)	- 5.5	5
Neck Coil Domains	**Kin1 Neck Coil** (345-405)	AEEWKRRYEKEKEKNARLKGKVEKLEIELARW RAGETVKAEEQINMEDLMEASTPNLEVEAS	(+13, -16)	- 3.0	5.0
	KIF1A Neck Coil (369-393)	IRELKDEVTRLRDLLYAQGLGDITD	(+4, -6)	- 2.1	4.7
	KIF1A NC+CC1 (369-523)	IRELKDEVTRLRDLLYAQGLGDITDMTNALVG MSPSSSLSALSSRAASVSSLHERILFAPGSEE AIERLKETEKIIAELNETWEEKLRRTEAIRME REALLAEMGVAMREDGGTLGVFSPKKTPHLVN LNEDPLMSECLLYYIKDGVTRVGREDA	(+20, -28)	- 7.4	5.0

Figure S2: Charge of the neck coil domains impacts motor properties of KIF1A

A, Table of the different dimerization and neck coil domains used in this study with the sequence, total number of charged residues, net charge of the domain at pH 6.9 and the pI. Net charge and pI were calculated using (http://protcalc.sourceforge.net/)

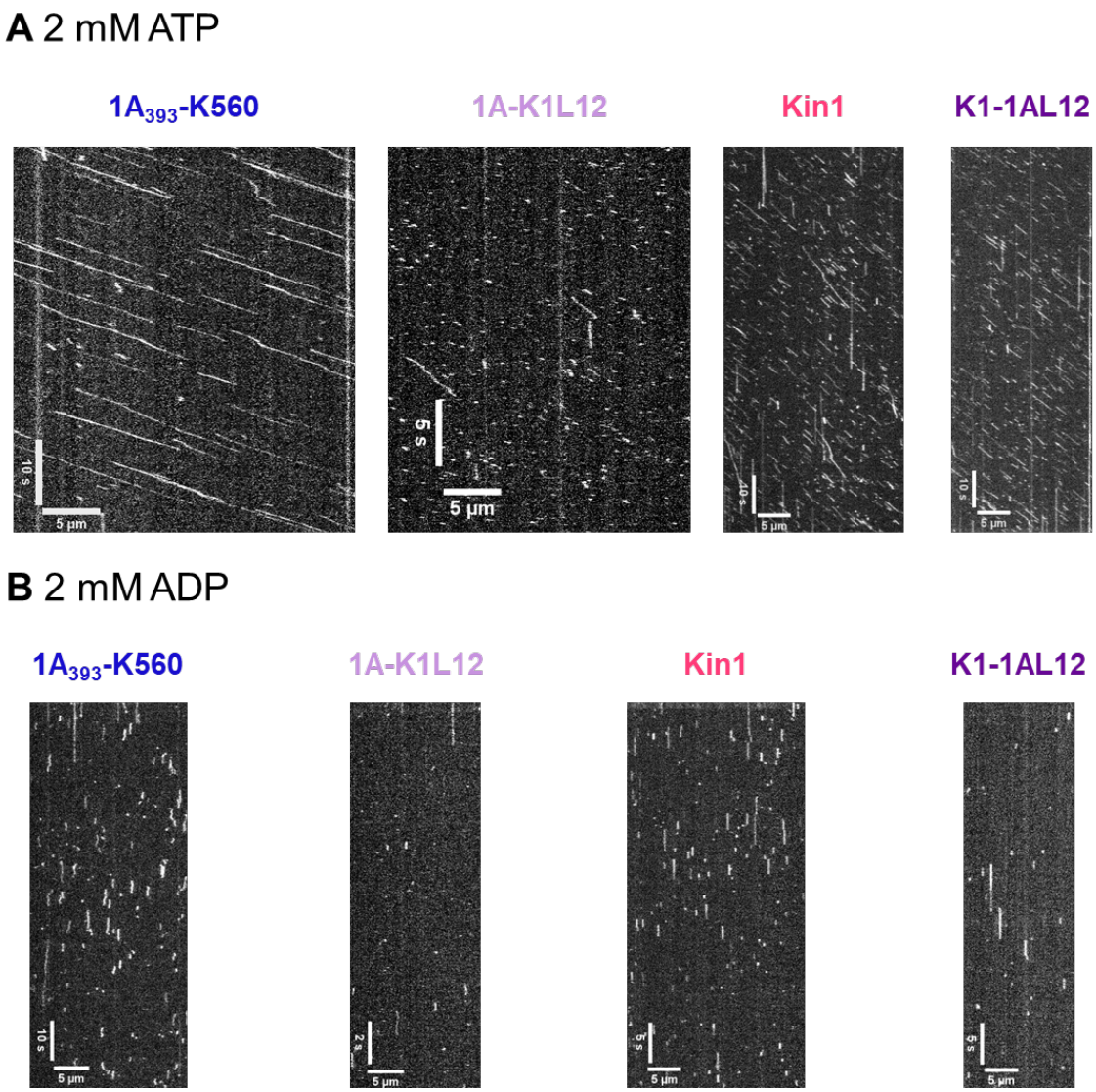

Figure S3: Example kymographs of constructs in ATP and ADP

A, Kymographs of different constructs used in Fig. 2, in 2 mM ATP and BRB80. **B**, Kymographs of different constructs used in Fig. 2, in 2 mM ADP and BRB80.

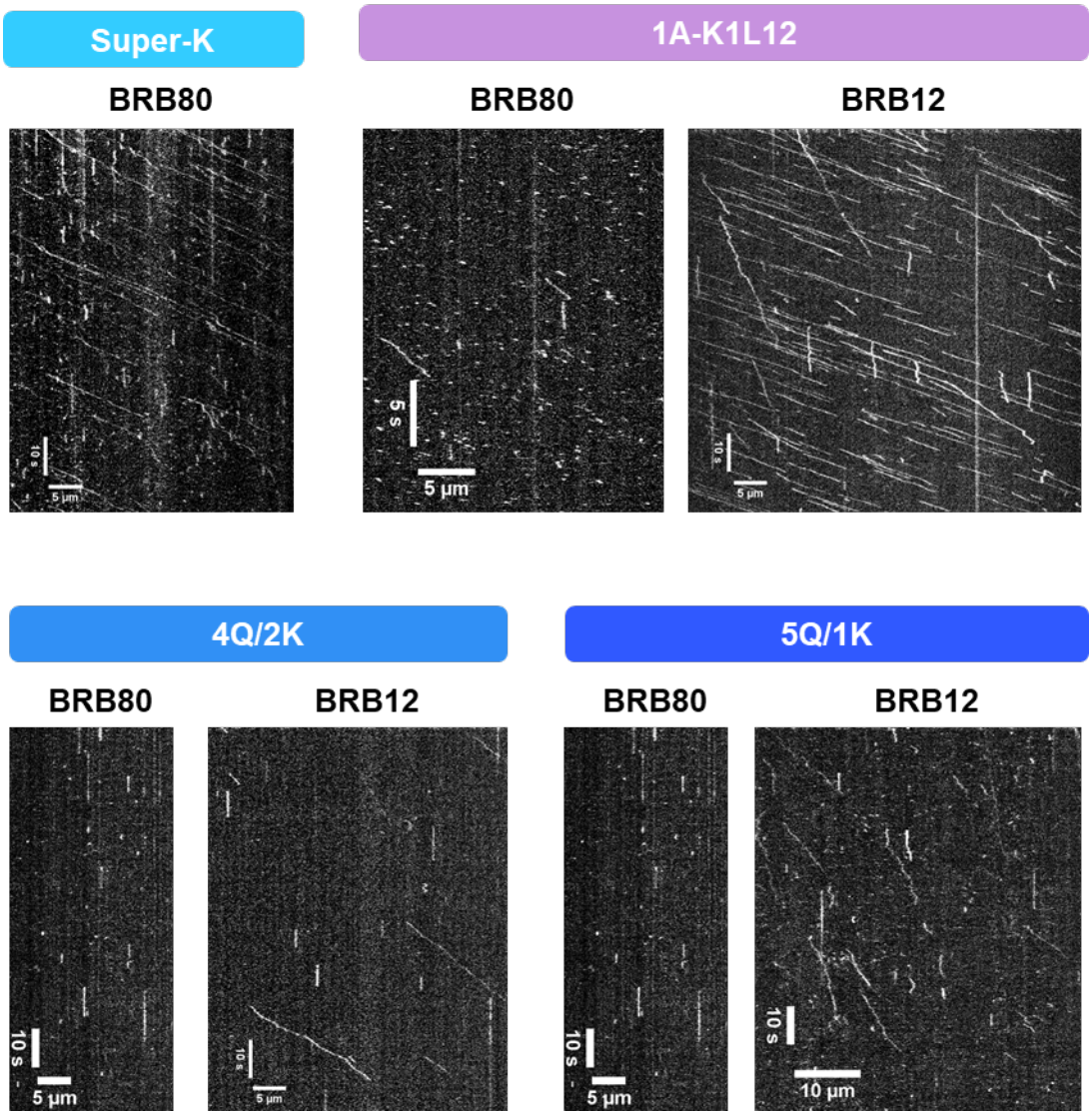

Figure S4: Example Kymographs of Charge Mutants in BRB80 and BRB12. Representative kymographs for the data presented in Figure 4.